Characterization and Meteorological Drivers of Dust Events over California's Central Valley

Precious Ebiendele[1] Adeyemi A. Adebiyi[1], John T. Abatzoglou[1], Karin Ardon-Dryer[2], Md. Minhazul Kibria[1] and Cade Hogle[2]

[1]School of Engineering, University of California, Merced, Merced, CA.

[2]Department of Geosciences, Atmospheric Science Group, Texas Tech

Abstract

Dust events in California's Central Valley pose severe risks to public health, regional air quality, and transportation. Yet, the climatology and meteorological drivers of dust events in the region are poorly characterized due to sparse monitoring and limitations of satellite observations. Using meteorological observations from 15 meteorological stations, we systematically catalog and analyze dust events across the Central Valley during 2005-2024, leveraging a hybrid approach that combines observer-reported dust codes with meteorological criteria that capture events missed by manual reporting. We identified 707 dust events, averaging ~35 events per year with a significant increase over the past two decades. These dust events are generally short-lived (≤1 h), occur mainly in the afternoon hours (14:00-18:00 local time), and are most frequent in the southern San Joaquin Valley between September and November. Self-organizing map analysis during the September-November peak dust season reveals four dominant synoptic-scale configurations driving dust events, characterized by anomalously strong surface winds, low relative humidity, and amplified mid-tropospheric troughs. Specifically, positively tilted troughs with northwesterly along valley surface winds produced widespread dust events during abnormally dry conditions, while negatively tilted troughs are associated with convective-driven fronts. Our results provide a robust foundation for improving dust forecasting and public health interventions in the agriculturally intensive Central Valley.

1. Introduction

Air pollution remains a significant challenge in California, particularly in the Central Valley, which includes several metropolitan areas ranked among the worst in the United States (US) for air quality (American Lung Association, 2025). The region frequently violates California and National Ambient Air Quality Standards for both fine particulate matter ($PM_{2.5}$) and ozone (e.g., EPA, 2018; SJVAPCD, 2025), resulting in severe public health impacts (e.g., Ha et al., 2024; Khanum et al., 2021; Wang et al., 2019; Zarate-Gonzalez et al., 2024) and impacts on agriculture (Zeeshan et al., 2024). Previous studies have shown that the Central Valley's severe air pollution results from the synergistic interactions of unfavorable topography, meteorology, and anthropogenic emissions (Chow et al., 2006; Zhao et al., 2011). Specifically, an enclosed basin bounded by the Sierra Nevada and Coast Ranges restricts horizontal air movement (e.g., Leighton, 1966; Young et al., 2016). This configuration leads to poor meteorological dispersion, particularly during stagnant high-pressure systems that promote inversions and trap pollutants near the surface (e.g., Beaver & Palazoglu, 2009; LaDochy & Witiw, 2023). Furthermore, these factors are exacerbated by anthropogenic emissions from agricultural activities, emissions from local and upwind transportation, oil and gas extraction, and urban centers (Almaraz et al., 2018; Angevine et al., 2013).

Unlike the conditions associated with chronic air quality issues in the Central Valley, characterized by stagnant air masses, dust storms have occasionally impacted the region during periods of strong winds, causing significant transportation hazards (Pauley et al., 1996), air quality concerns, and, in some cases, fatalities. Notably, California has experienced the highest number of dust-related fatalities among US states in recent decades (Tong et al., 2023). Recent dust events in the region have taken on varying forms, from the widespread dust storm on October 11, 2021, to a haboob-like event on November 11, 2024 (Fig. 1; NWS Hanford, 2024; Edwards, 2024). Dust events in the Central Valley, a semi-arid to Mediterranean-climate region, are primarily driven by wind erosion, where strong winds entrain and transport soil particles in the atmosphere (Zuo et al., 2024), drastically reducing visibility (Bhattachan et al., 2019). Specifically, the primary dust emission mechanism is saltation bombardment (Kok et al., 2012), where saltating sand grains over the surface bombard loose particles, breaking soil aggregates into smaller dust particles that are eventually ejected into the atmosphere (Gillette et al., 1979; Shao, 2008). In addition to the prevailing winds, dust emission also depends on environmental factors, including soil moisture, surface roughness, vegetation cover, and atmospheric stability (Hennen et al., 2023; Klose et al., 2014; Pu & Ginoux, 2017). These factors influence dust events in California's Central Valley, where unvegetated and agricultural lands are susceptible to wind erosion (e.g., Kolesar et al., 2022). Dust events have increased in the Central Valley in recent decades (Adebiyi et al., 2025; Evan et al., 2025; Tong et al, 2017), potentially by underlying changes in these environmental factors as well as changes in synoptic circulation patterns that frequently enhance surface winds and boundary-layer mixing.

The contributions of wind-blown dust and dust storms to the Central Valley's air pollution have often been underestimated (e.g., Cisneros et al., 2017; David et al., 2021). In addition, dust events in the Central Valley have been associated with Valley Fever (coccidioidomycosis) – a fungal lung infection caused by inhaling spores of the Coccidioides fungus, which primarily resides in agricultural soil (Tong et al., 2023). California has recently seen a significant increase in Valley fever cases, with reports rising from fewer than 1,000 in 2000 to a record high of 12,500 in 2024 (CDPH, 2025). Among these cases, the counties in the San Joaquin Valley (southern part of the broader Central Valley) consistently report the highest number of Valley Fever cases in the state.

Despite the critical consequences of dust events on public health, there is limited information in the literature about dust events in the Central Valley. These include the characterization of dust events and their synoptic drivers. In addition, there is a scarcity of monitoring stations capable of characterizing these dust events. Of the 20 active California Interagency Monitoring of Protected Visual Environments (IMPROVE) air quality monitoring stations used to measure fine dust concentrations (e.g., Hand et al., 2017), only one is in the middle of the Central Valley, where the majority of dust events occur (Ballard et al., 2008). While there are several Environmental Protection Agency (EPA), the California Air Resources Board (CARB), and local air districts monitoring stations that measure $PM_{2.5}$, very few measure PM_{10}, and these few stations cannot discriminate between dust and other coarse-mode pollutants that constitute PM_{10} (e.g., Chow et al., 1993). Even when available, these stations are far apart and often located near major cities, making it challenging to observe numerous small-scale dust events that are common in the rural agricultural areas of the Central Valley (Young et al., 2025). While remote-sensing observations from satellites have been used to detect dust events (Adebiyi et al., 2025; Ginoux et al., 2012), they are limited by their relatively coarse resolution (typically greater than 10 km) and by additional retrieval uncertainties, because satellite sensors do not directly observe dust under cloud cover (Castellanos et al., 2024).

To address this gap, we systematically catalog and characterize dust events in the California Central Valley using surface observations from Automated Surface Observation Systems (ASOS) and Automated Weather Observing Systems (AWOS) from 2005 to 2024. Unlike satellite or sparse IMPROVE networks, ASOS/AWOS reports high-temporal-resolution present-weather codes alongside meteorological measurements such as visibility, wind speed and gust, relative humidity, and event-triggered sub-hourly (SPECI) special reports, allowing precise timing of dust event duration even at night and under cloud cover. This automated station-based design also offers significant added value over historical dust storm catalogs, particularly the NOAA Storm Event Database (SED), due to reporting inconsistencies (Ardon-Dryer et al., 2023). Because SED dust reports rely on heterogeneous and non-standardized sources, they often misclassify dust events and leave significant spatial and temporal gaps.

Here, we quantify the climatology of dust events in the Central Valley, including their spatial and seasonal patterns. We also explore recent trends in dust events during 2005-2024 and their interannual relationships with drought conditions. Finally, we examine the meteorological patterns associated with dust events in the Central Valley. Efforts to identify large-scale meteorological patterns associated with dust events can help refine local forecasts and early warning systems to mitigate dust-related hazards. By systematically characterizing when, where, and how dust events develop in this region, this study aims to fill a current research gap and provide a foundation for improved dust event prediction, support targeted public health interventions, transportation safety policies, and control mitigation strategies as climate change and land-use pressures heighten regional dust activity.

2 Methods and Materials

2.1 Meteorological Observation Stations

Our study used station-based meteorological observations from the Automated Surface Observation System (ASOS) and Automated Weather Observing System (AWOS) networks operated by the U.S. National Weather Service and Federal Aviation Administration (Landolt et

al., 2019). As a result, these observing stations are often located at the airport and adhere to World Meteorological Organization (WMO) standards. These datasets comprise continuous quality-controlled surface weather observation stations across the US, and an array of sensors (see NOAA, 1998) produce these data, and the resulting sensor signals are processed using several automated algorithms (e.g., visibility algorithm, obscuration algorithm, single-site lightning sensor algorithm, and precipitation identification algorithm) that automatically report core Meteorological Aerodrome Report (METAR) elements (Cook et al., 2023; Landolt et al., 2019).

We used 15 meteorological stations (Table S1) spanning the Central Valley and covering 20 years from January 1st, 2005, to December 31st, 2024 (Fig. 2a). We obtained these datasets through a Python API from the Iowa Environmental Mesonet archive (https://mesonet.agron.iastate.edu) and converted them to local time. Each station reports visibility, wind speed and direction (including gusts), temperature, dew point, precipitation, sea-level pressure, and present weather codes (e.g., thunderstorms, rain, haze, and dust) at a time resolution of 5-minute to 1-hour intervals through METAR messages (Horel et al, 2002). We note that these stations report relative humidity (RH) at hourly intervals. To obtain sub-hourly RH, we computed RH at each METAR issuance time using the air temperature (T) and dew-point temperature (Td) encoded in the METAR text.

2.2 Identification of dust event

Although the ASOS/AWOS systems can automatically identify precipitation types and some obscurations, such as fog, they lack sensors to distinguish airborne dust from other particulate matter (NOAA, 1998). Instead, atmospheric dust particles affect these meteorological stations' measurements indirectly by reducing visibility, which the station may report as haze (HZ), unless an observer overrides it with a specific dust code (NOAA, 1998; Xi, 2020). These specific dust codes include "DU", which is widespread dust in the air; "BLDU", which is blowing dust at the station, resulting in an intermediate visibility drop of a few kilometers, DS, which are dust storms that typically reduce visibility to below about 1 km (WMO, 2019), and "SS", which are sandstorm. These dust codes are not automatically encoded in the record and require trained weather observers to enter each code manually. In practice, many of these stations operate in fully automated mode most of the time, using optical sensors that cannot distinguish dust from fog or haze, so dust events often go into the record without an explicit "dust" label, appearing only as lowered visibility with an HZ label as highlighted in Robinson & Ardon-Dryer, 2024.

Therefore, to adequately characterize all dust events at the stations, we selected dust cases using the following procedures (Figure S1): First, we selected all dust cases that were manually recorded with single weather codes, DU, BLDU, DS, and SS, as well as cases with other weather codes, but included these dust codes. Second, because not all dust events have recorded dust codes (e.g., the case study on November 11, 2024, which is recorded with an HZ label despite a visible dust event; see Fig. 1b-e), we also identified dust cases using observed meteorological parameters (Robinson & Ardon-Dryer, 2024). ASOS/AWOS automatically reports HZ as an obscuration during low visibility (<10km) and dry conditions (dew point depression > ~4°F) without precipitation, which is frequently observed in the Central Valley. Because HZ is not uniquely attributable to dust, using HZ alone may bias observer-coded dust frequency estimates. Therefore, we apply additional stringent criteria to treat HZ as dust (dusty-HZ) when it meets the meteorological conditions below: (a) Wind speed > 6 m/s; (b) Visibility drops < 10 km; and (c) RH < 70%. For these cases, we use a wind speed greater than 6 m/s because previous studies have suggested that this value is a realistic lower threshold for saltation and, by extension, dust uplift (Bagnold, 1941). In addition,

we used a visibility threshold of less than 10 km, as defined by the WMO (WMO, 2019), for blowing dust and dust storms. Further, we used RH less than 70% to remove cases that are associated with fog or widespread precipitation. In addition to the meteorological criteria, we further added an extra layer of screening for both (a) dusty-HZ cases that meet the meteorological conditions and (b) cases with manual dust codes (DU, DS, BLDU, SS). Specifically, we removed cases with any occurrence of wildfire smoke (FU) or mist (BR) conditions within a $\pm 2 hours$ window before and after the recorded drop in visibility to ensure that any reduction in visibility is most likely due to dust events (Suarez-Molina et al., 2024). Because wildfire smoke can mimic dust by reducing visibility during dry, windy conditions, we added an additional smoke-screening step. Beyond excluding cases with FU reported within $\pm 2 hours$ of visibility reduction, we examined wildfire and smoke reports and used the daily 10km wildfire smoke $PM_{2.5}$ dataset of Childs et al. (2022) as an extra screening data for cases in which no FU code was present. We treated elevated wildfire smoke ($PM_{2.5} \geq 20 \mu g m^{-3}$) over the station grid as evidence of possible smoke contamination and excluded cases when this coincided with reported wildfires or smoke reports.

In addition, we confirmed suspected dusty-HZ cases by leveraging the Geostationary Operational Environmental Satellite (GOES) Dust RGB product, National Weather Service (NWS) reports, as well as PM_{10} concentration measurements and smoke or wildfire-reported cases. GOES Dust RGB imagery was not a required part of the detection criteria, but rather a secondary confirmation tool applied only where available. Specifically, we visually assess the presence of dust plumes within one hour of each identified haze report using the goes2go Python library (Blaylock, B. 2023). This product is derived from the Advanced Baseline Imager (ABI), the primary imaging instrument onboard GOES-R series satellites and combines thermal infrared band differences (12.3-10.3μm and 11.2-8.4 μm) with the 10.3 μm brightness temperature to enhance the contrast of dust emissions relative to clouds and the surface (Kondragunta et al., 2020). However, because dust may not always be detectable in satellite imagery (e.g., due to cloud cover, low contrast, or timing differences), the absence of a visible plume did not rule out a case. We therefore reviewed NWS products, including Area Forecast Discussions and special weather statements. Any explicit mention of blowing dust, reduced visibility due to dust, or a blowing dust advisory in the surrounding region was treated as additional supporting evidence. Finally, we examined PM_{10} concentration at air quality stations closest to the ASOS/AWOS stations (Table S2) to assess if there was an increase ($PM_{10} \geq 35 \mu g m^{-3}$) during an identified dust episode (i.e., from the first identified dust-coded ASOS/AWOS report to the last dust-coded report, with an added $\pm$2-hour buffer to capture onset and end). With the above procedure, we identified 5,251 station-level dust observations, defined here as individual ASOS/AWOS reports (recorded at the station's native cadence) that were classified as dust based on the present weather codes (PWC) and /or our dusty-HZ screening criteria. Among these cases, 11.9% have at least one recorded dust code (i.e., DU, BLDU, DS, or SS), and the remaining 88.2% are dusty-HZ (Fig. 2).

We grouped dust observations into station-level dust events. A *dust event* at a station is defined as either (a) a single dust observation (visibility $\leq$ 10km), or (b) a sequence of consecutive dust observations at a station, evaluated at the station's native reporting cadence (e.g., 5-min or hourly), with no intervening non-dust observations. Observations included in an event must have visibility below 16km (including at least one observation with visibility $\leq$ 10km) and indicate dust either through dust codes (DU/BLDU/DS/SS) or dusty-HZ conditions. Thus, if a station records a single dust observation (visibility $\leq$ 10km), we retain it as a dust event of one reporting interval. To avoid

overcounting, we treat dust events that begin near midnight local time and persist into the following day as a single continuous event rather than two separate events. We also count as separate events if they occur at different times of the day and are separated by at least 2 hours (e.g., an event that occurs in the morning and another that occurs in the evening are counted as two separate events). We acknowledge, however, that some uncertainties remain in the identification of these multiple dust events within a single calendar day. For example, station reporting cadence and present-weather coding vary, and dust-related METAR code may be missing during the *intervening gap* (i.e., the period between the end of one dust event and the start of the next candidate dust event at the same station on the same calendar day). Therefore, an intervening gap without reported dust-related codes may not necessarily imply that dust was completely absent. In addition, it is also likely that one or more of the multiple dust events may be a sudden change in local conditions that satisfy our above-defined criteria before or after the main dust events. Despite these potential uncertainties, multiple dust events on the same calendar day at a given station are uncommon (~6% of days in which a station recorded an event contained more than one dust event). In addition, the mean period of the gap between dust events is about 383 minutes, and with mean characteristic relative humidity, visibility and wind speed that is different from the identified dust events (see Fig. S2). Characterization of identified dust is summarized at three levels: (a) dust observations: individual ASOS/AWOS reports meeting our dust criteria, (b) station-level dust events, and (c) station-level dusty days, defined as calendar days on which at least one dust event is recorded at a given station. The total number of identified dust events in the Central Valley is computed as the sum of station-level dust events across all stations over the study period (2005-2024), while the total number of station-level dusty days is computed as the total count of dusty days across all stations over the same period.

Trends in annual dust events were estimated using ordinary least squares regression applied to the regional annual time series (i.e., the number of dust events summed across all stations each year). Uncertainty is reported as ± 1 the standard error of the fitted slope. In addition, the statistical significance of the trend was assessed using a t-test on the regression slope. To check for consistency between our identified station-based dust event and satellite regional-scale measure of atmospheric dust loading, we estimated column-integrated dust burden following Adebiyi et al. (2025) using MODIS-derived dust optical depth.

2.3 Upper-Level Meteorological Information from Reanalysis Dataset

We used two complementary datasets to gain a deeper understanding of the synoptic patterns and drivers of dust events in California's Central Valley: the European Centre for Medium-Range Weather Forecasts' ERA5 reanalysis (Hersbach et al., 2020) and the North American Rapid Refresh version 3 (RAPv3; Benjamin et al., 2016). First, we use ERA5 to construct dusty-day composites of surface wind, relative humidity, 500-hPa geopotential height (z500), volumetric soil water in the surface layer (0-7cm), and total cloud cover at hourly resolution (2005 to 2024). For the composite analysis, we restrict the sample to *widespread dusty days*, defined as any day (UTC) when dust events were seen over at least 20% of stations in the Central Valley. We use this definition to reduce the influence of highly localized events that are unlikely to reflect a coherent synoptic-scale circulation. In addition, composite anomalies of dust-event meteorological drivers relative to climatology were computed, and the statistical significance of this difference was evaluated using a t-test, with statistical significance defined at $p < 0.05$.

Second, we further consider two diagnostic case studies (see Fig. 1; 11 October 2021 and 11 November 2024) using RAPv3 because it provides higher spatial resolution (13 km horizontal grid) and better resolves mesoscale gradients and near-surface wind maxima relevant for dust emission than the ERA5 reanalysis. RAPv3 uses the WRF-ARW model with a hybrid ensemble variational data assimilation scheme, ingesting frequent observations (e.g., radar reflectivity, cloud, and surface data). The benefits of high-resolution RAPv3 are that it can capture the evolution and spatial details of mesoscale dynamics in a rapidly changing atmosphere, such as small-scale frontal boundaries, sharp moisture–dryline interfaces, lee-side surface cyclogenesis, convective cold-pool surges, and jet streaks that entrain and transport dust. In contrast, ERA5's coarse resolution often smoothed out these features. We used only the initialization hours of RAPv3, and no forecast hours were used in this study. We obtained hourly geopotential height at 500 hPa (z500), relative humidity (RH500), 10m wind components (u10m, v10m), surface relative humidity, near-surface temperature, wind speed, and surface pressure. Although RAPv3 has a higher resolution than ERA5, we use ERA5 for our synoptic composite analysis because it provides a temporally consistent match with our selected meteorological stations over the period of interest (2005 to 2024). In contrast, RAP begins in 2012, while RAPv3 was implemented later in 2016.

2.4 Synoptic Pattern Classification: Self-Organizing Mapping (SOM)

We applied a self-organizing map (SOM) clustering algorithm, a machine-learning approach, to classify synoptic meteorological patterns associated with dust events in the Central Valley. We are motivated to use SOM because dust events in the Central Valley result from different combinations of large-scale synoptic patterns rather than a singular pattern. SOM maps high-dimensional input data onto a predefined number of cluster centers through an iterative training process (Kohonen, 2002). Several previous studies (Li et al., 2023; Sweeney et al., 2017; Uotila et al., 2017) have widely used this approach, including for capturing extreme events in data-limited contexts (Cassano et al., 2015). Unlike traditional clustering methods, its ability to preserve the topological relationships of the input data enables robust identification of recurring synoptic patterns (Sheridan & Lee, 2011).

Here, we used SOM to cluster z500 from ERA5 over the broader Northeast Pacific and western North America (30–50° N, 130–105° W) using the SOMoclu Python library (Wittek et al., 2017). We composited only widespread events (as defined in Section 2.3). For each day, we identified dust duration windows and computed the average daily dust window duration, which summarizes event persistence across the SOM nodes. We trained each SOM with an epoch size of 1000 and utilized a fixed random seed for reproducibility. After training, we identified the SOM's best-matching unit and assigned it to a single node label. We tested several SOM grid sizes (e.g., 4, 6, 8 clusters) and found that 4 clusters (Type 1–4) yielded distinctly interpretable patterns, whereas larger cluster sizes yielded redundant or transitional types. Of the identified widespread events, we then quantified the frequency of each synoptic pattern and computed composite geopotential fields by averaging all daily maps assigned to each type. In addition, spatial differences between types were evaluated using grid-point Welch's t-tests on the composite fields, with significance assessed at $p<0.05$.

2.5 Drought conditions

To examine how drought conditions modulate dust events under an identified synoptic scale pattern, we classify monthly dust events as a function of drought severity using the 1-month Standardized Precipitation-Evapotranspiration Index (SPEI-1) from the National Oceanic and Atmospheric Administration (NOAA) Climate Gridded Dataset (NClimGrid). Here, SPEI is based on standardized anomalies in monthly climatic water balance (P-PET, where P is precipitation and PET is potential evapotranspiration) using the Pearson Type III distribution. We spatially average SPEI-1 over the Central Valley to obtain a regional drought indicator. In addition, we classified months into drought categories using SPEI-1 thresholds (e.g., drought: SPEI< -0.8; abnormally dry: -0.79 $< SPEI < -0.50$; normal dry: -0.49$< SPEI < 0$, and no drought when SPEI > 0). To estimate the sensitivity of dust events to drought conditions, we defined annual dry-month frequency as the number of months per year with SPEI-1 < 0 and computed the Pearson correlation between annual dust event totals and annual dry-month frequency across the study period. Statistical significance was evaluated using a t-test, with $p<0.05$ considered significant.

To examine the timing of the first significant rainfall event in the Central Valley, we used daily precipitation from the gridMET (Abatzoglou, 2013) gridded meteorological dataset (1/24˚; ~4km resolution). Because precipitation over the valley is spatially heterogeneous, we identify rainfall onset using a spatial coverage metric. We first defined the onset of precipitation at both local and widespread scales. Locally, the onset for each grid cell was identified as the first Julian day after September 1, when precipitation reached at least 1 $mm\ day^{-1}$ on at least 2 of 3 consecutive days. At the regional scale, we defined a widespread onset date as the first day after September 1 on which at least 50% of Central Valley grid cells met this same criterion (Taylor et al., 2025). To avoid false onsets due to isolated early storms, we additionally required that at least one further widespread wet day (again, $\geq 50\%$ of grid cells receiving $\geq 1\ mm\ day^{-1}$) occur within the subsequent 14 days following the initial 3-day onset window. In addition, onset timing was expressed as days since 1 September and categorized into early and late onset using a median onset timing (i.e., 50th percentile of onset across the 2005-2024 period). Onsets occurring on or before the median were classified as early onset, and seasons with onsets occurring after the median were classified as late onset.

Furthermore, we quantified how dust is distributed across onset timing (early or late phase) and drought categories (e.g., no drought, normal dry, abnormally dry, and drought) by computing the fraction of dust events occurring in each onset-drought state. This describes how dust events are distributed across the timing phases of rainfall, conditional on dust occurrence.

Second, we assess whether drought conditions are associated with synoptic-scale patterns that drive dust in the Central Valley. Specifically, we asked whether the relative occurrence of the four SOM circulation types (Types 1-4) changes across dry conditions. To do this, we grouped dust events by SPEI drought categories and SOM type and quantified how the seasonal mix of SOM types (Types 1-4) varies.

3.0 Results

3.1 Verification of Dust Criteria using Recent Case Studies

To verify that our definition accurately captures the observed dust events, we show in Fig. 3 the evolution of wind speed, visibility, relative humidity, and PM_{10} for the two case studies identified in Fig. 1. As indicated in the section 2.2 above, we defined a dust event as a period when dust code is identified or when the wind speed is more than 6 m/s, visibility is less than 10 km, and relative

humidity is less than 70 %, if no specific dust code identified. Although not all are defined by dust codes, the above criteria identify a window of dust events that propagates southward in both cases. For the October 11, 2021 case, the northern station at Stockton (SCK) shows the dust event starts around 08:50 local time (LT), while the dust event starts about three hours later further south at Porterville (PTV; Fig. 3a). Satellite observations confirm that this dust event occurs between 08:00 and 19:00 LT, as it traverses north to south across the entire Central Valley (Fig. S3), as do station-based PM_{10} measurements. Unlike the October 11, 2021 case, the November 11, 2024 case was not visible from the remote-sensing platforms due to cloud cover associated with a propagating convective system (Fig. S4), but the dust storm preceding this system – a "haboob" – was captured by the ground-based cameras (see Fig. 1b). Specifically, for the November 11, 2024 case, the northern station at Merced (MCE) that captures the events starts around 12:25 LT, propagating southward through the Porterville (PTV) at 15:45LT (Fig. 3b). In the absence of satellite observation, we confirm this event by the ground-based EPA stations that shows sudden increases in PM_{10} measurements as the convective system and the haboob dust event travel southward (see purple lines in Fig. 3b). Overall, these results highlight the range of differences in dust events and the advantage of ground-based identification, especially when cloud cover prevents remote sensing.

3.2 Climatology of Dust Events in the Central Valley

Dust events in the Central Valley exhibit distinct annual, seasonal, and diurnal variabilities (Fig. 4). Between 2005 and 2024, we identify 660 station-level dusty day observations (~33 days yr^{-1}; Fig 2c). Most station-level dusty days occur in the southern San Joaquin Valley, with the highest numbers recorded at HJO (Hanford Municipal Airport) in Kings County and BFL (Meadows Field Airport) in Kern County, each averaging about 7 and 6 dusty days yr^{-1}, respectively (Fig. 2c). In addition, we further identified 707 station-level dust events corresponding to ~ 35 events yr^{-1} (Fig. 4a) as defined in section 2.2. We find that, relative to the average during the period of record, annual dust event frequency in the Central Valley has statistically significant 4.4% increase/yr during 2005-2024 (Fig. 4a; $p<0.05$). In addition, we also find that the correlation between annual dust events and annual frequency of drought conditions (monthly SPEI values less than 0) is 0.56 ($p < 0.05$). While lack of rainfall is generally prevalent in the Central Valley, this result suggests that drought conditions play a role in the interannual variability of dust events in the Central Valley (see section 3.5 below). Consequently, the annual variability of station-based dust-event counts is consistent with satellite-based estimates of column-integrated dust burden, suggesting that our station-based assessment of dust events is representative of the entire Central Valley (see blue line in Fig. S5). However, the relationship between annual dust burden and SPEI classes is not strictly linear and may reflect lagged hydroclimatic effects through vegetation cover and soil moisture (e.g., Schumacher et al. 2022; Eibedingil et al. 2024).

Second, we also find that the seasonal cycle shows a peak in the number of dust events in October (Fig. 4b). In addition, there is a secondary peak in dust events, with lower dust counts, in April-June. In addition, this seasonal cycle of our identified dust events is consistent with the PM_{10} measurements recorded at locations near the identified ASOS/AWOS stations (Fig. S6). Similar to the stations' dust counts, the PM_{10} measurements show a peak concentration in October, approximately 91.3 μgm^{-3} during the dust events identified in Fig. 4, compared to the climatology of 53.6 μgm^{-3} in the same month. For this seasonal cycle of dust events crossing the Central Valley, wind speed is an important predictor, with its influence modulated by other parameters (see next

section and Fig. 5). For example, stronger winds during the core rainy season are likely to produce fewer dust events because precipitation, higher soil moisture, and increased vegetation cover reduce surface erodibility and suppress dust emission. In contrast, the fall peak can be associated with the transition from quiescent to more dynamic synoptic circulation patterns (see section 3.4 below) with seasonally dry soils prior to the onset of winter precipitation (Lukovic et al., 2021) and potentially compounded by seasonal farming activities (e.g., harvest, post-harvest).

Third, we also find that most of the dust events in the Central Valley occur during the daytime, with the peak between 14:00 and 18:00 LT (Fig. 4c). This peak period also corresponds to the peak daily temperature and resultant convective boundary layer turbulence, resulting in stronger surface winds that are conducive to dust mobilization (Zhang et al., 2024). Regardless of the time of day of the dust event, we find that about 78% of all identified dust events in the Central Valley occur for one hour or less (Fig. 4d). Dust events exceeding five hours constituted only 1.4% of total occurrences, with exceptionally long events (>10 hours) exceedingly rare (1.7%). This characterization of dust-event durations is largely consistent across all stations, with short-duration dust events (≤ 1 hr) ranging from ~50% to 89% of all occurrences, and high-duration dust events (> 1 hr) ranging from 11% to 50% of all occurrences (Fig. S7). In addition, higher numbers of long-duration dust events occur more in the southern stations, where there are more overall dust occurrences (see Fig. 2). For example, 30.4% and 23.9% of dust events in BFL and HJO, respectively, are long-duration events (Fig. S7). Overall, the dominance of short-duration events across stations is consistent with other reported studies in different dust-prone regions, such as the southwestern United States (Robinson & Ardon-Dryer, 2024) and Phoenix, Arizona (Sandhu et al., 2024).

3.3 Local Meteorological Characteristics of Dust Events

In addition to the distinct annual, seasonal, and diurnal variability, dust events also exhibit unique local meteorological characteristics that differ from the baseline climatology during the same period across stations in the Central Valley (Fig. 5). Our result confirms that dust events occur during higher wind speeds, even when typical conditions are calmer (Fig. 5a & d). On average, wind speed during dust events is 8.2 $m\,s^{-1}$, which is significantly higher than the climatology value of 2.6 $m\,s^{-1}$ (Fig. 5a).

In addition to the wind speed, our result also shows that visibility and RH are generally significantly lower during dust events than climatological conditions (Fig. 5). Specifically, we find that, on average, the visibility is lower by 7.9 km and the RH by 22.1 % during dust events than the climatology across the stations in the Central Valley. While most dust events occur during higher wind speeds, lower visibility, and RH than climatology, a small fraction occur at wind speeds less than 6 m/s, visibility higher than 12 km, and RH higher than 70%. Our analysis indicates that all of these remaining cases are associated with defined dust codes (such as BLDU, DU, DS, and SS). Because our screening thresholds were applied only to hazy-dust cases in the absence of dust codes (see Fig. S1), these coded events were identified independently of the screening criteria and may occasionally occur without a strong signal in screening variables.

The spatial distribution of these meteorological characteristics during dust events shows substantial station-to-station variability across the Central Valley (Fig. 5d-f). Several stations in the southern part exhibit generally higher wind speeds and lower RH during dust events. While the strongest wind speeds during dust events occur at the Redding (RDD) in the north, this location is likely influenced by mesoscale factors as wind accelerates through mountain gaps into the Valley (see Fig. 2a), rather than large-scale synoptic drivers (see section 3.4 below). In addition,

five of the eight stations in the southern part of the Central Valley have mean visibility less than 7 km during dust events compared to only two in the northern part of the Central Valley. Like wind speed, there is less spatial variability in mean RH in the southern than in the northern parts of the Central Valley.

3.4 Synoptic-scale Assessment of Dust Events in the Central Valley

Like the station-based meteorological characteristics above, we also examine the differences between the composite-mean of dust events and baseline climatology using ERA5 reanalysis. We find that the differences across the entire Central Valley are statistically significant, similar to those characterized by the meteorological stations (Fig. 6). Specifically, dust events are typically associated with stronger wind speeds and lower RH than the climatology (Fig. 6a & b). Both station-level and valley-wide diagnostics indicate a similar fingerprint but different amplitude, with larger station-level anomalies ($\Delta U = +5.6 m/s$; $\Delta RH = -22.1\%$; Fig 5) compared to the valley basin mean composite ($\Delta U = +1.67 m/s$; $\Delta RH = -13.90\%$; Fig 6), as expected because station-level anomalies were computed for dust events at individual stations, whereas valley-wide anomalies were based on composites of dust events occurring anywhere within the central valley. The changes in wind speed and RH are linked to synoptic forcing associated with a mid-tropospheric trough just north of California. Consistent with this pattern, dust events are accompanied by lower 500-mb geopotential height than the baseline climatology (Fig. 6c). During the fall months with the highest dust events (September-November), this type of system often dominates the synoptic-scale pattern, influencing the meteorological characteristics that are conducive to dust mobilization (Fig. S8).

3.4.1 Synoptic Categorization of Dust Events in the Central Valley

Our SOM analysis yielded four (4) dominant synoptic configurations (Types) that influence widespread dusty days in the Central Valley (Fig. 7). The first configuration, representing 35.6% of dust events (Type 1), shows a negatively tilted mid-tropospheric trough with the low-pressure center over the northeastern Pacific Ocean, northwest of California (Fig. 7a & Fig S9). SOM mode 4 (Type 4; accounting for 15.3% of dust events) also features a negatively tilted trough, but with the low-pressure center over the Cascade Range. In contrast, Types 2 and 3 are both positively tilted mid-tropospheric troughs, each accounting for 28.8% and 20.3% of dust events, respectively. Although both low-pressure centers are north-eastward of California, Type 2 has its low-pressure center positioned further east, tilting it slightly more than Type 3. Unrelated to the tilt axis of the geopotential fields, Type 1 and Type 3 are also associated with stronger pressure gradients at 500 mb than Type 4, with Type 2 showing similarly strong gradients. In addition, the synoptic configuration patterns (Fig. 7a) codified in z500 are significantly different ($p<0.05$) between Type 1 and Type 4, and between Type 2 and Type 3 across much of the domain.

These differences in pressure gradient, tilt, and overall synoptic-scale configuration among the configuration Types are linked to specific wind speed and direction at the surface, which influence dust events (Fig. 7b-d and Fig. S10). Specifically, the average wind speeds for Type 2 and Type 3 are higher than those of Type 1 and Type 4. This is partly due to the orientation and direction of surface winds, as well as the influence of the surrounding topography. For Type 1 and Type 4, the winds are mainly westerly (with some southwesterlies in Type 1 and northwesterlies in Type 4). In contrast, the winds for Type 2 and Type 3 tend to be more north-northwesterly, aligning more closely with the orientation of the Central Valley. Because the valley is bounded by the Coastal

Range to the west and the Sierra Nevada to the east, these mountain barriers can help channel the low-level flow along the valley axis (Zhong et al., 2004; Zaremba et al., 1999), which is consistent with stronger valley-wide surface winds seen in Types 2 and 3. These differences in flow pathway can be attributed to how Sierra Nevada and Coastal Ranges redirect large scale atmospheric flow, consequently, enhancing low-level winds along the Central Valley, with a greater proportion exceeding 6 m/s (the threshold for dust mobilization), than those in Type 1 and Type 4 synoptic configurations.

In addition to the enhanced surface winds, these synoptic-scale configurations are also associated with soil and atmospheric conditions that favor dust events. Specifically, we find that soil and atmospheric conditions for Type 2 and Type 3 are drier than for Type 1 and Type 4 (Fig. 8 and Fig. S10). This contrast is consistent with differences in flow direction and associated air-mass characteristics. Types 2 and 3 are characterized by predominantly northerly to northwesterly flow, which is typically associated with dry continental air masses and reduced moisture availability over California. In contrast, Types 1 and 4 exhibit a stronger westerly flow, which allows more marine influence from the Pacific.

While the Central Valley generally has drier soil than other parts of the state (Fig. S10b), the anomalies for Type 1 and Type 4 show that soil water is higher than the September-November climatology in northern California and some parts of the Central Valley. Unlike Type 4, which shows positive soil water anomalies concentrated in northern California (including the northern Central Valley), Type 1 shows positive anomalies mainly along far northern California, with much of the Central Valley generally neutral or drier than climatology. In contrast, soil water in the San Joaquin Valley and other southern parts of California is drier than the September-November Climatology. This suggests that most of the dust events in Type 1 are more likely to occur in the San Joaquin Valley than in the Sacramento Valley. Conversely, Type 2 and Type 3 have drier soil water conditions throughout most of the Central Valley. Within the Central Valley, the driest soil regions largely overlap with areas of predominantly strong wind speeds in the Sacramento Valley, indicating that synoptic-scale configurations of Type 2 and Type 3 are most likely to facilitate dust events in the Sacramento Valley.

Using RH and cloud cover as proxies, our results further show a consistent pattern of atmospheric moisture across the Central Valley and the state, similar to soil water distribution. The RH for Type 2 and Type 3 is generally lower than for Type 1 and Type 4. Additionally, Type 1 and Type 4 also show anomalously higher cloud cover than Type 2 and Type 3 when compared to the September-November climatology. This, along with the anomalous increases in RH and soil water, suggests that the likelihood of precipitation is higher in Type 1 and Type 4 than in Type 2 and Type 3. The explanation for this is that Type 1 and Type 4 dust events typically occur in synoptic environment with greater maritime influence, likely associated with nearby or approaching troughs that enhance onshore flow. This will typically increase relative humidity and cloud cover compared with Type 2 and Type 3. For Type 1 and Type 4 events, the process of dust emission and associated dust events are less likely to be widespread across the Central Valley. For example, dust events could be linked to the frontal passage of convective systems, where wind speeds facilitate dust emission, especially when the soil is dry, particularly in the San Joaquin Valley (Pauley et al., 1996).

3.4.2 Examples of the dominant synoptic-scale patterns.

To further illustrate the predominant patterns of synoptic-scale configurations associated with dust events, we consider the two case studies: October 11, 2021 and November 11, 2024 dust events (Fig. 9). Based on the SOM classification (see section 2.4; Fig 7a & Fig S9), the October 11 case is more representative of Type 2 and Type 3 with a largely (neutrally to) positively tilted trough, whereas the November 11 case is more representative of Type 1 and Type 4 with a predominantly negatively (to neutrally) tilted trough (Fig. 9).

For the October 11, 2021 case (Fig. 9a), our results show that the positively tilted 500-mb geopotential height propagates eastward from 05:00 LT, when the low-pressure center is directly north of California, to 14:00 LT, when the low-pressure center intensifies and moves over neighboring Nevada. This intensification causes the tilt of the trough to change significantly, roughly transitioning from a synoptic configuration similar to Type 2 at 05:00 LT to Type 3 by 11:00 LT (compare Fig. 9 and Fig. 7). Additionally, like Type 2, strong winds (greater than 6 m/s) first concentrate in the Sacramento Valley. As the low-pressure center moves eastward and pressure gradients over California strengthen, these strong winds expand to cover the entire Central Valley, leading to widespread dust emission (see Fig. S3), aided by the dry soil and atmospheric conditions (Fig. S11). Stations recorded strong winds as the event propagated southward, along with a significant reduction in visibility and relative humidity (Fig. 3).

In contrast, for the November 11, 2024 case (Fig. 9b), the result shows a negatively tilted 500-mb geopotential height, with the low-pressure center offshore over the Pacific Ocean before 10:00 LT and propagating eastward over the Pacific Northwest by 19:00 LT. Additionally, a precipitation band accompanies this synoptic configuration and moves southward at a similar timescale to the upper-level system (Fig. S4). This synoptic-scale pattern, with associated precipitation and cloud distribution over California and the Central Valley, exhibits all the characteristics of Type 1 and Type 4 described above (Fig. 9 and Fig. 7). Unlike the October 11 case, which featured clear skies and widespread dust emission, the November 11 event appears to be triggered by the cold pool or gust fronts at the precipitation boundary and detected by the meteorological stations (see Fig. 1b & Fig. 3b) coincident with dry soils (Fig. S10).

3.5 Relationships between fall dust events and drought

While synoptic-scale systems drive dust events in California, drought severity can modulate how readily those systems produce dust by preconditioning the land surface (Achakulwisut et al., 2017). By separating dust events into different drought categories, we find that most dust events occur during abnormally dry to drought conditions, accounting for about 56% of dust events regardless of the season (Fig. 10a). The mean precipitation onset date (i.e., the first significant rainfall event across the Central Valley) shows a clear north-south gradient, with earlier onset in the northern Central Valley and later onset in the southern San Joaquin Valley (Fig. S12). Consistent with this pattern, the fall dust events were most frequent when the onset of widespread precipitation was late, and drought conditions were normal-dry, with such conditions accounting for the largest fraction of SON dust events (35%, Fig. S13). However, a substantial fraction of SON dust events occurs in early-onset years under abnormally dry (17%) and normal-dry (15%) conditions (Fig. S13).

Furthermore, to link the September-November synoptic types to hydroclimate variability, we group dust events by SPEI drought category and compute the type composition (Fig. 10b). The synoptic-scale configurations as drought categories show that Type 1 and Type 4 occur more frequently during no-drought (63%) and normal-dry (70%) conditions than in abnormally dry

(33%) or drought (45%) conditions. In addition, the percentage contribution of Type 2 and Type 3 collectively increases from no-drought (37%) and normal-dry (30%) conditions compared to abnormally dry (67%) and drought (55%) conditions. This relationship between drought categories and the synoptic-scale configuration is consistent with the earlier SOM results (Fig. 7-8). Specifically, Type 1 and Type 4, which occur more during no-drought and normal-dry conditions, are associated with higher relative humidity and cloud cover and have a higher chance of precipitation than Type 2 and Type 3, which occur more during abnormally dry and drought conditions. Overall, these findings suggest that drought state and the timing of precipitation modulate dust likelihood by setting land-surface susceptibility, while the dominant synoptic circulation types identified (Fig. 7a & Fig S9) govern the wind flow that transports dust in the Central Valley.

4.0 Discussion and Conclusions

This study provides the first known effort to characterize the climatology and meteorological drivers of dust events in California's Central Valley. First, our analysis indicated that dust is more frequent in the southern valley and has significantly increased over the past two decades (2005-2024). In addition, Central Valley dust events exhibit a bimodal seasonal pattern, a dominant fall peak (September-November) and secondary spring peak (April-May), partly attributed to local surface desiccation following the cessation of the growing season for annuals (e.g., post-harvest activities and lack of irrigation) and harvest season for perennials. For example, tomato harvest and processing typically span early July through October in the Central Valley (USDA NASS, 2024), and field operations during this period may disturb soils and increase exposed, erodible surfaces. Similar disturbances occur during almond harvest (August through October), which involves mechanical tree shaking followed by sweeping and pickup operations that generate substantial PM_{10} emissions in the San Joaquin Valley (Faulkner, 2013). Furthermore, the strong bimodal seasonal pattern of dust events in the Central Valley, with a fall maximum, contrasts with the unimodal pattern of dust from desert sources of the western United States, which typically peaks in the spring (Hand et al., 2017), and the one found for California in Ardon-Dryer et al. 2023.

Second, dust events in the Central Valley tend to peak during the late afternoon and early evening hours, consistent with the diurnal maximum in boundary-layer mixing and near-surface wind variability, mirroring similar patterns in neighboring dust-prone regions (Raman et al., 2014; Sandhu et al., 2024). This timing also implies potential compounding with commute hours, which is notable given that dust events frequently reduce visibility below 10 km (Ashley et al., 2015; Bhattachan et al., 2019). Furthermore, more cases of valley fever are occurring in California's Central Valley, particularly in the Southern San Joaquin Valley (Cooksey, 2020), where our results show that dust events are more common. Coccidioides fungi thrive in dry soils and can be easily aerosolized during typical dust events, increasing the risk of exposure, especially among farm workers (McCurdy et al., 2018). Coupled with the increase in dust events over the past two decades (2005-2024), this trend poses additional public health concerns.

Third, our SOM clustering demonstrated that dust events in the Central Valley are driven by distinct synoptic configurations that are characterized by pronounced pressure gradients, which organize low-level flow and influence notable differences in dust transport pathways. In addition, these identified patterns further suggest that the surrounding topography, particularly the Coast Ranges and the Sierra Nevada, plays a significant role in how dust can be sustained and

redistributed along the valley. We find that among these widespread pathways, the two predominant patterns characterized by eastward low-level flow closely follow synoptic patterns that produce eastward winds, which carry dust from the Central Valley toward the Sierra Nevada. The eastward transport of dust can have significant implications for the Sierra Nevada snowpack for winter or spring dust-on-snow events. Studies have shown that dust deposition in Sierra snowpack significantly reduces albedo and radiative forcing, accelerating snowmelt timing and altering runoff timing and water availability (Huang et al., 2022).

While dust in the Central Valley follows a particular synoptic-scale pattern, land use and surface conditions, especially agricultural practices, control its sources. A significant proportion of the valley plain is cultivated agricultural land. However, due to a combination of drought and long-term declines of groundwater, portions of the Valley have been left fallow, potentially increasing soil surface erodibility. A recent study revealed that about 77% of these fallowed agricultural lands in California are in the San Joaquin Valley (Adebiyi et al., 2025) and thus provide potential environments for dust emissions even under moderate wind conditions. In addition, disturbed surfaces such as construction sites, unpaved roads, and dry lakebeds could serve as dust sources in the valley. Drought and land use change are tightly coupled with dust emissions (Tegen et al., 2004; Aryal & Evans, 2021), and an intensification of this coupled system in the region can reduce available soil moisture and potentially expose the soil surface. In addition, broader future projections for the southwestern US (including the Central Valley) under a warming climate indicate drier conditions, which could increase the likelihood of dust events (Pu & Ginoux, 2017).

Despite the potential direct impacts that dust events have on human health and transportation, advisories and warnings for dust impacts are quite rare in the Central Valley. For example, the NWS offices in the Central Valley sparingly issued advisories or warnings for dust during the 20-year period of our study, suggesting that such hazards are not well codified from a forecasting perspective. This highlights the value of translating the catalog dust events information compiled here into a transferable warning framework that can support NWS operations. Specifically, the meteorological characteristics and synoptic patterns that modulate dust events identified in this study will provide actionable inputs for a simple dust-risk indicator that could help forecasters and end users anticipate periods of reduced visibility and elevated particulate exposure. We find that preferred large-scale meteorological patterns coincident with dry soils are key for widespread dust events. Forecasting efforts based on pattern recognition, along with more sophisticated measures (Sarafian et al., 2023), may aid in the development of early warning systems for dust events that can allow vulnerable populations to take protective measures and mitigate against reducing traffic accidents.

While this study offers a comprehensive characterization of dust event dynamics across California's Central Valley, we note several caveats. Our dust detection algorithm relies on ASOS/AWOS data, which, despite its high temporal resolution, is subject to known observational biases. These data are retrieved from a sparse network of airport stations and can sometimes miss short-lived convective outflows that did not pass through those stations. Only about 11% of the dust events in our database were explicitly tagged with associated dust codes (DU, BLDU, DS) by trained observers. Additionally, because temporal changes in manual coding practices could in principle influence dust count, we note this as a potential source of uncertainty. While our dust detection algorithm offers added value in capturing dust activity that observers did not record, we likely do not fully capture the scale of dust events herein. In addition, the confirmatory sources (PM_{10} measurements, NWS discussions, smoke/wildfire reports, and GOES satellite imagery)

have some inherent data challenges: the required PM_{10} temporal period (2005-2024) was not available for all 15 stations; NWS discussions varied in spatial detail; and satellite detection is affected by cloud cover and the timing of overpass. These limitations mean that independent confirmation sources were not always available for every candidate's events. Thus, the reported dust event presented should be interpreted as a conservative estimate, reflecting the limitations of available monitoring systems in fully capturing short-lived, spatially localized, or low-intensity episodes. In addition, we acknowledge that there may contain small number of false-positive cases where dust like conditions were flagged but could not be fully verified because supporting confirmatory sources were unavailable or incomplete.

Overall, our study significantly contributes to how regional and synoptic-scale processes interact to shape dust climatology in complex agricultural basins like California's Central Valley. These findings have direct implications for water resource management, air quality forecasting, public health assessments, and transportation safety risk, potentially allowing communities in the Central Valley to develop adaptation strategies to prepare for these events, especially as climate-driven shifts in drought severity and land use continue to modulate these events.

Acknowledgments
We thank Caitlin Scully and ALERTCalifornia UC San Diego for providing videos for our case studies. Karin Ardon-Dryer and Cade Hogle's work was supported by a National Science Foundation grant (Grant #2235913). Cade Hogle would also like to thank the Honors College Undergraduate Research Scholars Program, supported by The CH Foundation and the Helen Jones Foundation, Inc., at Texas Tech University, for his undergraduate research funding support.

Funding:
The study was supported by the U.S. Department of Energy (DOE) Climate Resilience Center (#DE-SC0024238).

Competing interests:
The authors declare that they have no competing interests

Data availability
All data used in this study are publicly available. Meteorological Aerodrome Reports (METARs) obtained are available at the Iowa University Mesonet (https://www.mesonet.agron.iastate.edu/request/download.phtml?network=CA_ASOS, Iowa Mesonet, 2025). The ERA5 reanalysis data used is available from the Copernicus Climate Data Store at https://cds.climate.copernicus.eu/datasets (last accessed on 08-11-2025). Hourly PM_{10} data used is available from EPA (https://aqs.epa.gov/aqsweb/airdata/download_files.html#Raw). SPEI is obtained from the National Oceanic and Atmospheric Administration (NOAA) Climate Gridded Dataset (NClimGrid) (https://www.ncei.noaa.gov/). We retrieve precipitation from GridMET dataset (Abatzoglou, 2013; https://www.climatologylab.org/gridmet.html). Wildfire and smoke PM is available at (Childs et al 2022; https://www.stanfordecholab.com/wildfire_smoke). The North American Rapid Refresh version 3 (RAPv3; Benjamin et al., 2016) data used is available at https://registry.opendata.aws/noaa-rap/ . Code and workflow used in this analysis is available at a dedicated GitHub repository https://github.com/precious95/Synoptic-DustEvents_CentralValley.

References

Abatzoglou, J. T. (2013). Development of gridded surface meteorological data for ecological applications and modelling [Dataset]. International Journal of Climatology, 33(1), 121–131. https://doi.org/10.1002/joc.3413

Achakulwisut, P., Shen, L., & Mickley, L. J. (2017). What controls springtime fine dust variability in the western United States? Investigating the 2002–2015 increase in fine dust in the US Southwest. Journal of Geophysical Research: Atmospheres, 122(22), 12-449.

Adebiyi, A. A., Kibria, M. M., Abatzoglou, J. T., Ginoux, P., Pandey, S., Heaney, A., & Akinsanola, A. A. (2025). Fallowed agricultural lands dominate anthropogenic dust sources in California. *Communications Earth & Environment*, *6*(1), 324.

ALERTCalifornia UC San Diego, Kuester, F., Aaron, E., Blair , S., Bormann, J., Brady , R., Brust, A., Conley, J., Connolly,J.,Davis, G., Driscoll , J., Eakins, J., Hagadorn, A., Hoban, B., Holmes, J., Hui, N., Liu, C., Lo, E., McAvoy, S., McFarland, C., Nicholson, C., Norton, B., Norton, T., Papatrechas, T., Peach, C., Petrovic, V., Richards, L., Rissolo, D., Scully, C., Veik, D., Vernon, F., Wells , Z., Williams, M. Driscoll, N. (2025). ALERTCalifornia Camera Archive https://doi.org/10.34946/D6X306

Almaraz, M., Bai, E., Wang, C., Trousdell, J., Conley, S., Faloona, I., & Houlton, B. Z. (2018). Agriculture is a major source of NO x pollution in California. Science advances, 4(1), eaao3477.

American Lung Association. (2025). *State of the Air 2025* (American Lung Association, 2025).

Angevine, W. M., Brioude, J., McKeen, S., Holloway, J. S., Lerner, B. M., Goldstein, A. H., ... & Bon, D. (2013). Pollutant transport among California regions. Journal of Geophysical Research: Atmospheres, 118(12), 6750-6763.

Ardon-Dryer, K., Gill, T. E., & Tong, D. Q. (2023). When a dust storm is not a dust storm: Reliability of dust records from the storm events database and implications for geohealth applications. GeoHealth, 7(1), e2022GH000699.

Aryal, Y. N., & Evans, S. (2021). Global dust variability explained by drought sensitivity in CMIP6 models. Journal of Geophysical Research: Earth Surface, 126(6), e2021JF006073.

Ashley, W. S., Strader, S., Dziubla, D. C., & Haberlie, A. (2015). Driving blind: Weather-related vision hazards and fatal motor vehicle crashes. *Bulletin of the American Meteorological Society*, *96*(5), 755-778.

Bagnold, R.A. (1941). The physics of blown sand and desert dunes. Springer Netherlands. https://doi.org/10.1007/978-94-009-5682-7

Ballard, M., Newcomer, M., Rudy, J., Lake, S., Sambasivam, S., Strawa, A. W., ... & Skiles, J. W. (2008). Understanding the correlation of San Joaquin air quality monitoring with aerosol optical thickness satellite measurements. In ASPRS Annual Conference, Baltimore MD.

Beaver, S., and A. Palazoglu, 2009: Influence of synoptic and mesoscale meteorology on ozone pollution potential for San Joaquin Valley of California. Atmos. Environ., 43, 1779–1788.

Benjamin, S. G., Weygandt, S. S., Brown, J. M., Hu, M., Alexander, C. R., Smirnova, T. G., ... & Manikin, G. S. (2016). A North American hourly assimilation and model forecast cycle: The Rapid Refresh. Monthly Weather Review, 144(4), 1669-1694.

Bhattachan, A., Okin, G. S., Zhang, J., Vimal, S., & Lettenmaier, D. P. (2019). Characterizing the role of wind and dust in traffic accidents in California. GeoHealth, 3(10), 328-336.

Blaylock, B. K. (2023). GOES-2-go: Download and display GOES-East and GOES-West data (Version 2022.07.15) [Computer software]. https://github.com/blaylockbk/goes2go

California Department of Public Health. (2025). Valley fever in California Year-end Data Dashboard. (Dashboard data last updated July 1, 2025). Retrieved 29, 2025 from https://www.cdph.ca.gov/Programs/CID/DCDC/Pages/ValleyFeverDashboard.aspx

Cassano, J. J., E. N. Cassano, M. W. Seefeldt, W. J. Gutowski Jr., and J. M. Glisan (2016), Synoptic conditions during wintertime temperature extremes in Alaska, J. Geophys. Res. Atmos., 121, 3241–3262, doi:10.1002/2015JD024404.

Castellanos, P., Colarco, P., Espinosa, W. R., Guzewich, S. D., Levy, R. C., Miller, R. L., ... & Yu, H. (2024). Mineral dust optical properties for remote sensing and global modeling: A review. Remote Sensing of Environment, 303, 113982.

Childs, M.L., Li, J., Wen, J., Heft-Neal, S., Driscoll, A., Wang, S., Gould, C.F., Qiu, M., Burney, J. and Burke, M., 2022. Daily local-level estimates of ambient wildfire smoke PM2. 5 for the contiguous US. Environmental Science & Technology, 56(19), pp.13607-13621.

Chow, J. C., Chen, L. W. A., Watson, J. G., Lowenthal, D. H., Magliano, K. A., Turkiewicz, K., & Lehrman, D. E. (2006). PM2. 5 chemical composition and spatiotemporal variability during the California Regional PM10/PM2. 5 Air Quality Study (CRPAQS). Journal of Geophysical Research: Atmospheres, 111(D10).

Chow, J. C., Watson, J. G., Lowenthal, D. H., Solomon, P. A., Magliano, K. L., Ziman, S. D., & Richards, L. W. (1993). PM10 and PM2. 5 compositions in California's San Joaquin Valley. Aerosol Science and Technology, 18(2), 105-128.

Cisneros, R., Brown, P., Cameron, L., Gaab, E., Gonzalez, M., Ramondt, S., ... & Schweizer, D. (2017). Understanding public views about air quality and air pollution sources in the San Joaquin Valley, California. Journal of Environmental and Public Health, 2017(1), 4535142.

Cook, N. J. (2023). Impact of ASOS real-time quality control on convective gust extremes in the USA. Meteorology, 2(2), 276-294.

Cooksey, G. L. S., Nguyen, A., Vugia, D., & Jain, S. (2020). Regional analysis of coccidioidomycosis incidence—California, 2000–2018. MMWR. Morbidity and mortality weekly report, 69.

David, L. M., Ravishankara, A. R., Brey, S. J., Fischer, E. V., Volckens, J., & Kreidenweis, S. (2021). Could the exception become the rule? "Un-controllable'' air pollution events in the U.S. due to wildland fires. Environmental Research Letters. https://doi.org/10.1088/1748-9326/abe1f3

Eibedingil, I. G., Gill, T. E., Kandakji, T., Lee, J. A., Li, J., & Van Pelt, R. S. (2024). Effect of spatial and temporal "drought legacy" on dust sources in adjacent ecoregions. Land Degradation & Development, 35(4), 1511-1525.

Edwards, A. (2024). Extreme dust storm halts traffic, cuts power in California's Central Valley, *San Francisco Chronicle*, 11 November. Available at: https://www.sfchronicle.com/weather/article/california-central-valley-dust-storm-19907604.php

EPA, 2018. Current nonattainment counties for all criteria pollutants, United States Environmental Protection Agency. Available at: https://www3.epa.gov/airquality/greenbook/ancl.html , Accessed date: 2 October 2025.

Evan, A.T., Adebiyi, A.A., Burney, J., Chen, S.-H., Chen, W., D'Odorico, P., Fischella, M., Heaney, A., Hoyer, K., Kok, J., Lybrand, R., Okin, G., Porter, W., Rinaldo, T., & Zender, C.S. (2025, April). Beyond the haze: A UC Dust report on the causes, impacts, and future of dust storms in California [Report]. UC Dust, Scripps Institution of Oceanography, University of California, San Diego. https://ucdust.ucsd.edu/wp-content/uploads/sites/492/2025/04/UC-Dust-Report-2025.pdf

Faulkner, W. B. (2013). Harvesting equipment to reduce particulate matter emissions from almond harvest. Journal of the Air & Waste Management Association, 63(1), 70-79.

Gillette, D. A., Adams, J., Endo, A., & Smith, D. (1979). Environmental factors affecting dust mobilization by wind erosion. Saharan Dust: Mobilization, Transport, Deposition. SCOPE Rep, 14, 27-48.

Ginoux, P., Prospero, J. M., Gill, T. E., Hsu, N. C., & Zhao, M. (2012). Global-scale attribution of anthropogenic and natural dust sources and their emission rates based on MODIS Deep Blue aerosol products. Reviews of Geophysics, 50(3).

Ha, S., Abatzoglou, J. T., Adebiyi, A., Ghimire, S., Martinez, V., Wang, M., & Basu, R. (2024). Impacts of heat and wildfire on preterm birth. Environmental research, 252, 119094.

Hand, J. L., Gill, T. E., & Schichtel, B. A. (2017). Spatial and seasonal variability in fine mineral dust and coarse aerosol mass at remote sites across the United States. Journal of Geophysical Research: Atmospheres, 122(5), 3080-3097.

Hennen, M., Chappell, A., & Webb, N. P. (2023). Modelled direct causes of dust emission change (2001–2020) in southwestern USA and implications for management. Aeolian Research, 60, 100852.

Hersbach, H., Bell, B., Berrisford, P., Hirahara, S., Horányi, A., Muñoz-Sabater, J., et al. (2020). The ERA5 global reanalysis. *Quarterly Journal of the Royal Meteorological Society*, 146(730), 1999–2049. https://doi.org/10.1002/qj.3803

Horel, J., Splitt, M., Dunn, L., Pechmann, J., White, B., Ciliberti, C., Lazarus, S., Slemmer, J., Zaff, D., & Burks, J. (2002). Mesowest: Cooperative mesonets in the western United States. Bulletin of the American Meteorological Society, 83(2), 211–226.

Huang, H., Qian, Y., He, C., Bair, E. H., & Rittger, K. (2022). Snow albedo feedbacks enhance snow impurity-induced radiative forcing in the Sierra Nevada. Geophysical Research Letters, 49(11), e2022GL098102.

Iowa Environmental Mesonet (2025). ASOS-AWOS-METAR Data Download, https://www.mesonet.agron.iastate.edu/request/download.phtml?network=CA_ASOS

Khanum, S., Chowdhury, Z., & Sant, K. E. (2021). Association between particulate matter air pollution and heart attacks in San Diego County. Journal of the Air & Waste Management Association, 71(12), 1585-1594.

Klose, M., Shao, Y., Li, X., Zhang, H., Ishizuka, M., Mikami, M., & Leys, J. F. (2014). Further development of a parameterization for convective turbulent dust emission and evaluation based on field observations. Journal of Geophysical Research: Atmospheres, 119(17), 10441–10457.

Kohonen, T. (2002). The self-organizing map. Proceedings of the IEEE, 78(9), 1464-1480.

Kok, J. F., Parteli, E. J. R., Michaels, T. I., & Karam, D. B. (2012). The physics of wind-blown sand and dust. Reports on Progress in Physics, 75(10), 106901.

Kolesar, K. R., Schaaf, M. D., Bannister, J. W., Schreuder, M. D., & Heilmann, M. H. (2022). Characterization of potential fugitive dust emissions within the Keeler Dunes, an inland dune field in the Owens Valley, California, United States. Aeolian Research, 54, 100765.

Kondragunta, S., I. Laszlo, H. Zhang, P. Ciren, and A. Huff. (2020). Air quality applications of ABI aerosol products from the GOES-R series. In The GOES-R series, 203–17. Elsevier. doi: 10.1016/B978-0-12-814327-8.00017-2.

LaDochy, S., & Witiw, M. (2023). California Weather and Air Pollution. In Fire and Rain: California's Changing Weather and Climate (pp. 185–196). Springer.

Landolt, S. D., Lave, J. S., Jacobson, D., Gaydos, A., DiVito, S., & Porter, D. (2019). The impacts of automation on present weather–type observing capabilities across the conterminous United States. Journal of Applied Meteorology and Climatology, 58(12), 2699–2715.

Leighton, P. A. (1966). Geographical aspects of air pollution. Geographical Review, 151–174.

Li, J., Wong, M. S., & Nazeer, M. (2023). Integrating physical index and self-organizing mapping for aerosol dust detection (PISOM) over Himawari-8 AHI satellite images. *Atmospheric Environment*, *309*, 119921.

Luković, J., Chiang, J. C., Blagojević, D., & Sekulić, A. (2021). A later onset of the rainy season in California. Geophysical Research Letters, 48(4), e2020GL090350.

McCurdy, S. A., Portillo-Silva, C., Sipan, C. L., Bang, H., & Emery, K. W. (2020). Risk for coccidioidomycosis among Hispanic farm workers, California, USA, 2018. Emerging Infectious Diseases, 26(7), 1430.

National Weather Service San Joaquin Valley/Hanford. (2024). *Storm Data and Unusual Weather Phenomena – November 2024*. NOAA/NWS.

NOAA, 1998: *Automated Surface Observing System (ASOS) user's guide*. National Weather Service Doc., 38 pp., https://www.weather.gov/media/asos/aum-toc.pdf.

NOAA. (2025). National centers for environmental information, Climate monitoring. https://www.ncei.noaa.gov/access/monitoring/products/, last accessed in August 2025.

Pauley, P. M., Baker, N. L., & Barker, E. H. (1996). An observational study of the "Interstate 5" dust storm case. Bulletin of the American Meteorological Society, 77(4), 693-720.

Pu, B., & Ginoux, P. (2017). Projection of American dustiness in the late 21st century due to climate change. Scientific Reports, 7(1), 5553.

Raman, A., Arellano, A. F., & Brost, J. J. (2014). Revisiting haboobs in the southwestern United States: An observational case study of the 5 July 2011 Phoenix dust storm. Atmospheric Environment, 89, 179–188. https://doi.org/10.1016/J.ATMOSENV.2014.02.026

Robinson, M. C., & Ardon-Dryer, K. (2024). Characterization of 21 years of dust events across four West Texas regions. *Aeolian Research*, *67*, 100930.

San Joaquin Valley Air Pollution Control District. Ambient air quality standards and Valley attainment status. Retrieved August 23, 2025, from https://www.valleyair.org/air-quality-information/ambient-air-quality-standards-valley-attainmnet-status/

Schumacher, D. L., Keune, J., Dirmeyer, P., & Miralles, D. G. (2022). Drought self-propagation in drylands due to land–atmosphere feedbacks. Nature Geoscience, 15(4), 262-268.

Sandhu, T., Kelley, M., Rawlins, E., & Ardon-Dryer, K. (2024). Identification of dust events in the greater Phoenix area. Atmospheric Pollution Research, 15(11), 102275. https://doi.org/10.1016/j.apr.2024.102275

Sarafian, R., Nissenbaum, D., Raveh-Rubin, S., Agrawal, V., & Rudich, Y. (2023). Deep multi-task learning for early warnings of dust events implemented for the Middle East. NPJ climate and atmospheric science, 6(1), 23.

Shao, Y. (Ed.). (2008). Physics and modelling of wind erosion. Dordrecht: Springer Netherlands.

Sheridan, S. C., & Lee, C. C. (2011). The self-organizing map in synoptic climatological research. Progress in Physical Geography, 35(1), 109-119.

Suarez-Molina, D., Cuevas, E., Alonso-Pérez, S., Cana, L., Montero, G., & Oliver, A. (2024). Dust events characterization from visibility, trends, and Dust Adversity Index in the Canary Islands for 1980–2022. *Heliyon*, *10*(10).

Sweeney, A., Loikith, P., & Lintner, B. (2017). Characterizing Large-Scale Meteorological Patterns and Associated Temperature and Precipitation Extremes over the Northwestern United States Using Self-Organizing Maps. *Journal of Climate*, 30, 2829-2847. https://doi.org/10.1175/JCLI-D-16-0670.1.

Taylor, G. P., Loikith, P. C., Lee, H. K., Rahimi, S., & Hall, A. (2025). Historical and future autumn rain and wind onset over western North America using regional climate models. Journal of Geophysical Research: Atmospheres, 130(21), e2025JD044267.

Tegen, I., Werner, M., Harrison, S. P., & Kohfeld, K. E. (2004). Relative importance of climate and land use in determining present and future global soil dust emission. Geophysical Research Letters, 31(5).

Tong, D. Q., Gill, T. E., Sprigg, W. A., Van Pelt, R. S., Baklanov, A. A., Barker, B. M., Bell, J. E., Castillo, J., Gassó, S., & Gaston, C. J. (2023). Health and safety effects of airborne soil dust in the Americas and beyond. Reviews of Geophysics, 61(2), e2021RG000763.

Tong, D. Q., Wang, J. X. L., Gill, T. E., Lei, H., & Wang, B. (2017). Intensified dust storm activity and Valley fever infection in the southwestern United States. Geophysical Research Letters, 44(9), 4304–4312.

Uotila, P., Perkins-Kirkpatrick, S., Pepler, A., Gibson, P., & Alexander, L. (2017). On the use of self-organizing maps for studying climate extremes. *Journal of Geophysical Research: Atmospheres*, 122, 3891 - 3903. https://doi.org/10.1002/2016JD026256.

U.S. Department of Agriculture, National Agricultural Statistics Service. (2024, August 29). 2024 California processing tomato report. https://www.nass.usda.gov/Statistics_by_State/California/Publications/Specialty_and_Other_Releases/Tomatoes/2024/202408ptom.pdf

Wang, T., Zhao, B., Liou, K.-N., Gu, Y., Jiang, Z., Song, K., Su, H., Jerrett, M., & Zhu, Y. (2019). Mortality burdens in California due to air pollution attributable to local and nonlocal emissions. Environment International, 133, 105232.

WMO (World Meteorological Organization). (2019). WMO technical regulations annex II manual on codes international codes. I. 1.

Wittek, P., Gao, S. C., Lim, I. S., & Zhao, L. (2017). Somoclu: An efficient parallel library for self-organizing maps. *Journal of Statistical Software*, *78*, 1-21.

Xi, X. (2020). Global aeolian dust variations and trends: a revisit of dust event and visibility observations from surface weather stations. Atmospheric Chemistry and Physics Discussions, 2020, 1–34.

Young, B. N., Tryner, J., Hernandez Ramirez, L., WeMott, S., Erlandson, G., Li, X., Kuiper, G., Dean, D. A., Martinez, N., & Phillips, M. (2025). Particulate Matter Pollution in an Agricultural Setting: A Community-Engaged Research Study. Environments, 12(10), 348.

Young, D. E., Kim, H., Parworth, C., Zhou, S., Zhang, X., Cappa, C. D., Seco, R., Kim, S., & Zhang, Q. (2016). Influences of emission sources and meteorology on aerosol chemistry in a polluted urban environment: results from DISCOVER-AQ California. Atmospheric Chemistry and Physics, 16(8), 5427–5451.

Zarate-Gonzalez, G., Brown, P., & Cisneros, R. (2024). Costs of air pollution in california's san joaquin valley: A societal perspective of the burden of asthma on emergency departments and inpatient care. Journal of Asthma and Allergy, 369–382.

Zaremba, L. L., & Carroll, J. J. (1999). Summer wind flow regimes over the Sacramento Valley. Journal of Applied Meteorology, 38(10), 1463-1473.

Zeeshan, N., Freer-Smith, P., Murtaza, G., Wong, A. E., & Taylor, G. (2024). His dark materials: quantifying the problem of dust (particulate matter) in the agricultural landscape of California. Atmospheric Environment, 330, 120562.

Zuo, X., Zhang, C., Zhang, X., Wang, R., Zhao, J., & Li, W. (2024). Wind tunnel simulation of wind erosion and dust emission processes, and the influences of soil texture. International Soil and Water Conservation Research, 12(2), 455–466.

Zhang, L., Zhang, H., Cai, X., Song, Y., Mamtimin, A., & He, Q. (2024). Physical mechanisms of deep convective boundary layer leading to dust emission in the Taklimakan Desert. Geophysical Research Letters, 51(10), e2024GL108521.

Zhao, Z., Chen, S.-H., Kleeman, M. J., Tyree, M., & Cayan, D. (2011). The impact of climate change on air quality–related meteorological conditions in California. Part I: present time simulation analysis. Journal of Climate, 24(13), 3344–3361.

Zhong, S., Whiteman, C. D., & Bian, X. (2004). Diurnal evolution of three-dimensional wind and temperature structure in California's Central Valley. Journal of Applied Meteorology, 43(11), 1679-1699.

FIGURES

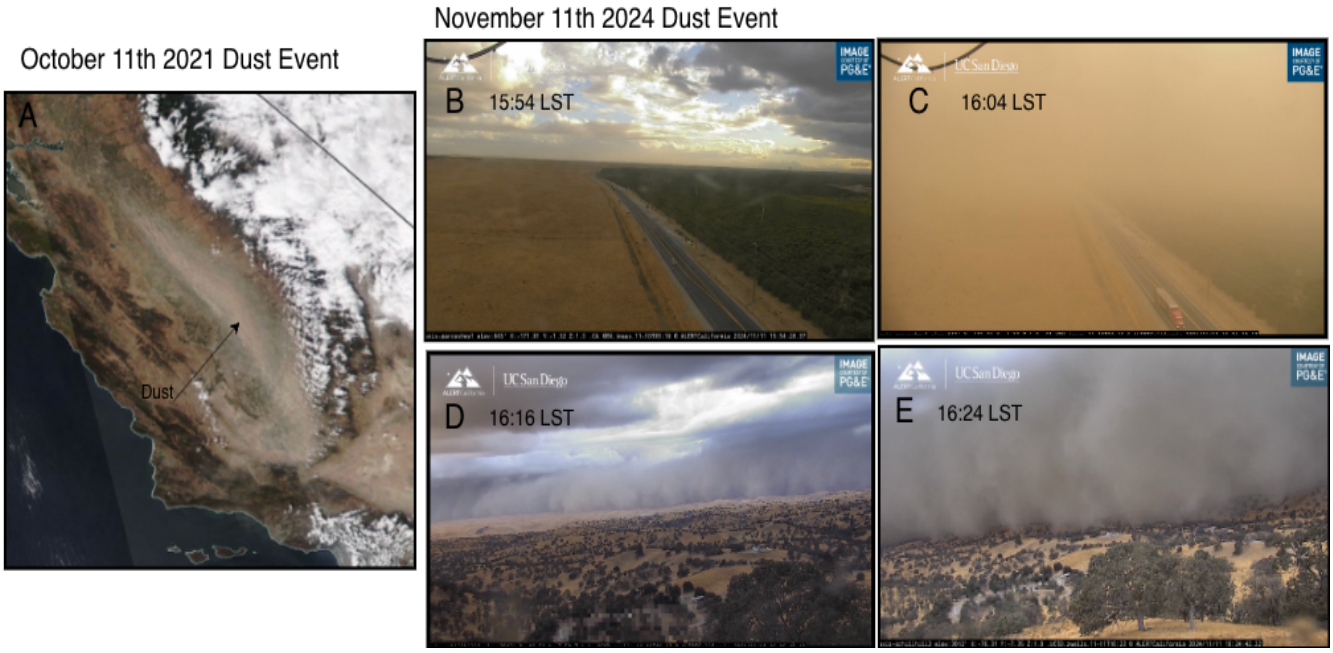

Fig 1. Satellite and ground-based view of two California Central Valley dust events. (a) The true-color satellite image for October 11, 2021, from NASA Worldview, shows a widespread along-valley dust event. (b-e) The UC San Diego ALERTCalifornia camera (2025) network (in Kern County, along Garces Highway (b & c) and Southern Sierra foothills/Kern County (d & e) during the November 11, 2024, haboob dust event, showing conditions before (b, d) and during (c, e) the dust passage.

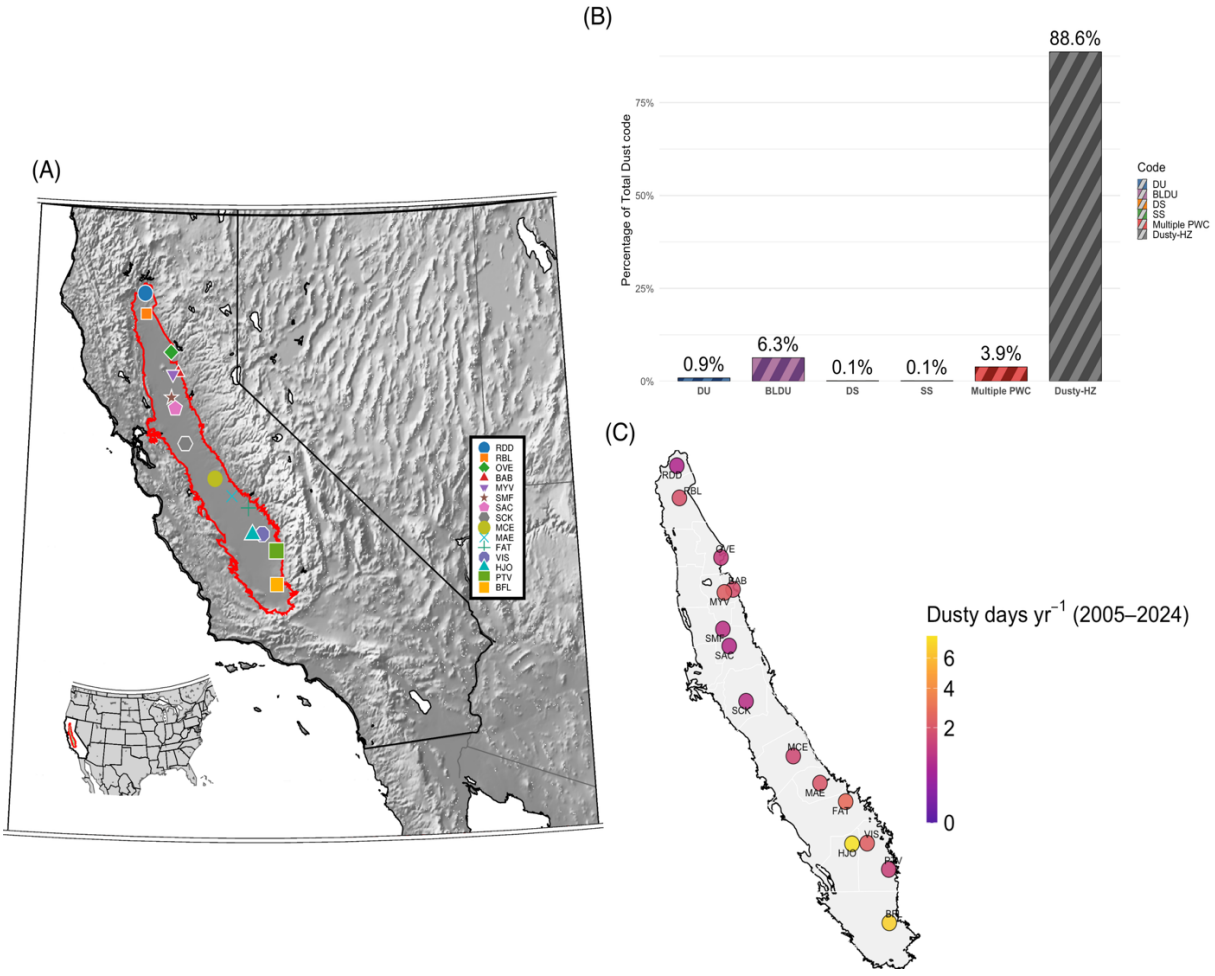

Fig 2. Dust occurrence across the California Central Valley. (a) Study area map showing the Central Valley (red outline) and 15 meteorological stations (see details of the stations in Table S1) (b) Percentage fraction of dust-related present weather codes (PWC) reported across all stations from 2005-2024. Codes are DU (Widespread dust), BLDU (blowing dust), DS (dust storm), SS (sandstorm), Multiple PWC (report of more than one dust related code) and Dusty-HZ (dusty haze conditions under dry, strong windy and reduced visibility conditions) (c) 20-year annual average of station-level dusty days.

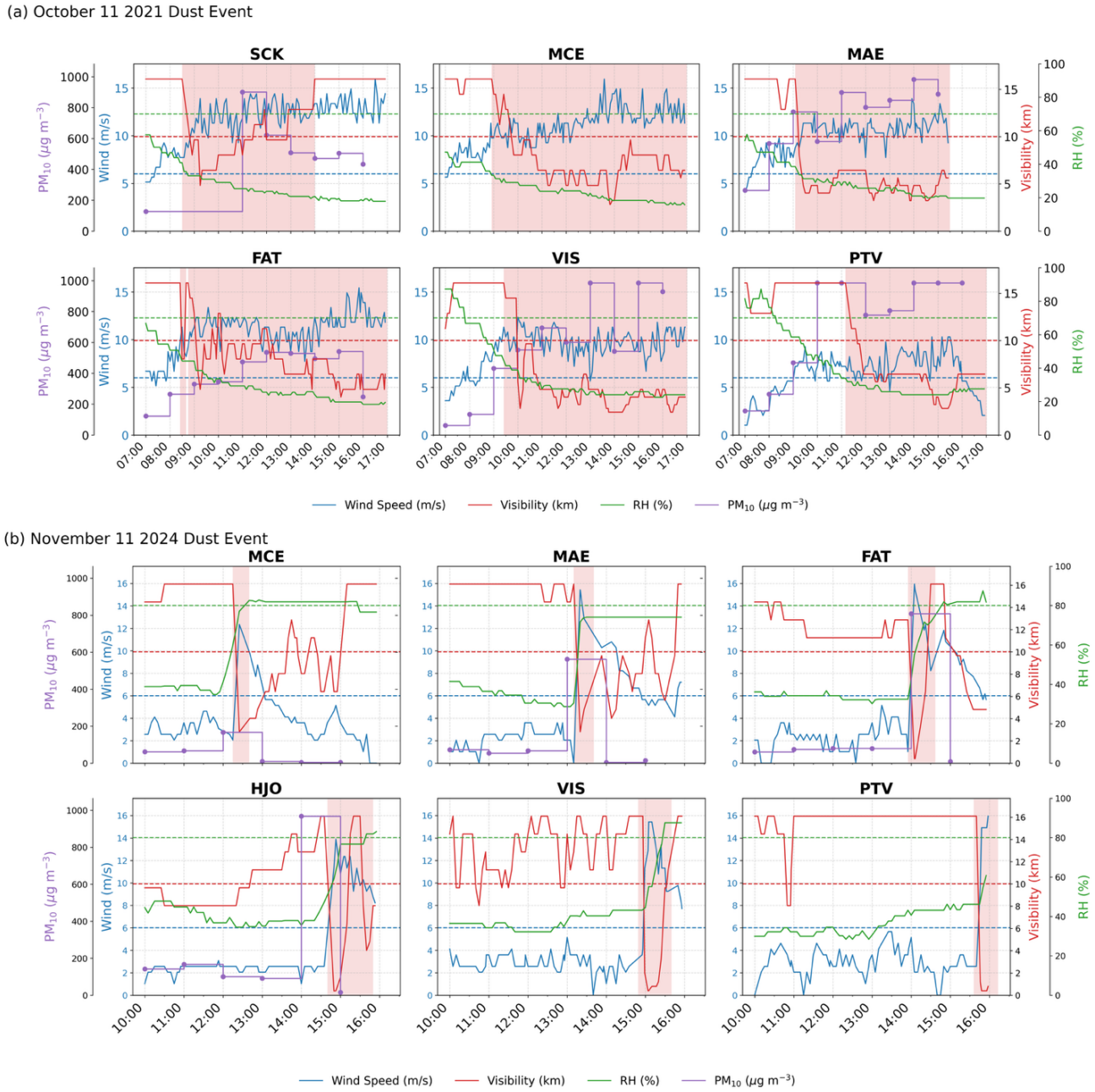

Fig 3. Wind speed (blue lines), visibility (red lines), and relative humidity (green lines) during (a) October 11, 2021, (b) November 11, 2024, at meteorological stations. Associated hourly PM10 data from nearby stations are shown in purple lines. Highlighted in pink are dust events meeting the criteria described in section 2.2, with dashed horizontal lines showing thresholds of wind speed, visibility, and relative humidity used.

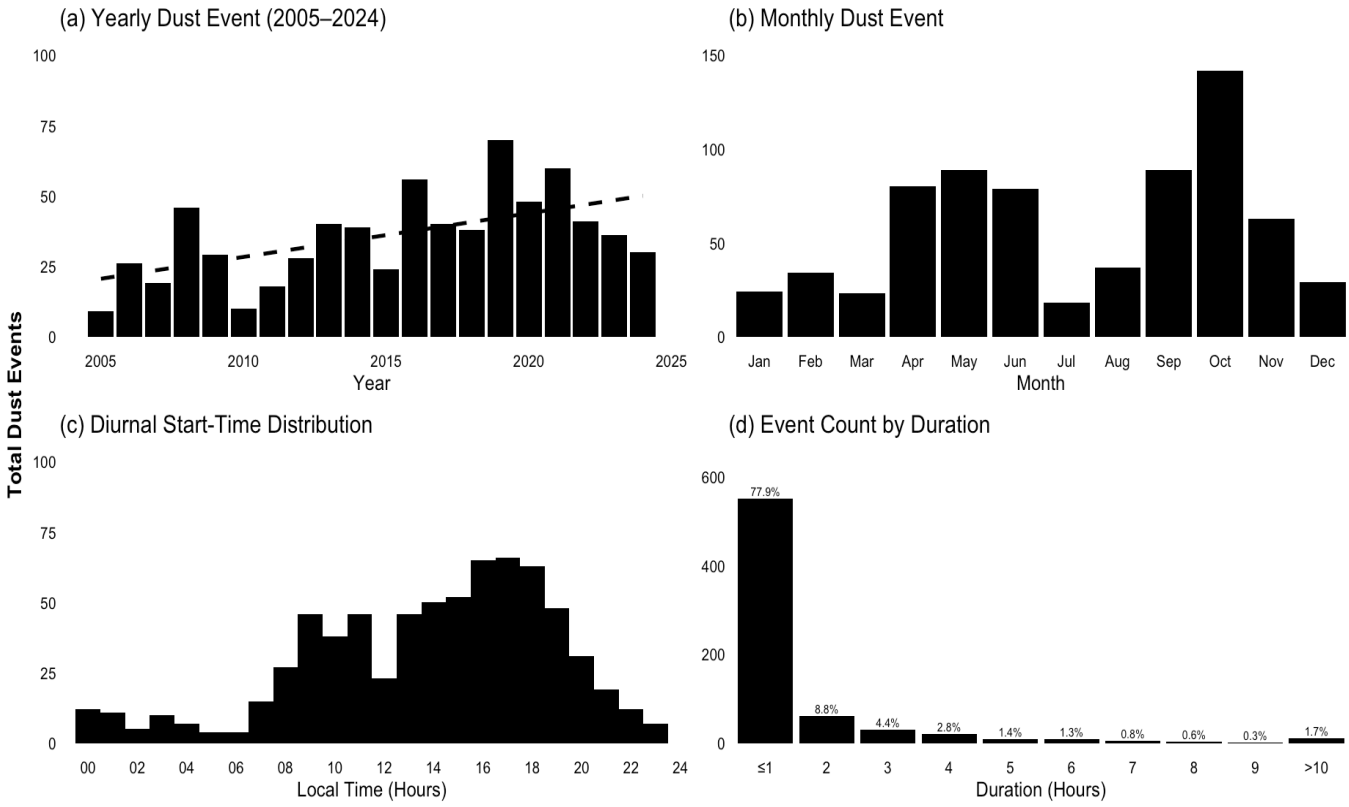

Fig 4. Temporal distribution of dust events in the Central Valley for 2005–2024. (a) Yearly distribution, (b) monthly distribution, (c) diurnal distribution, and (d) duration of dust events.

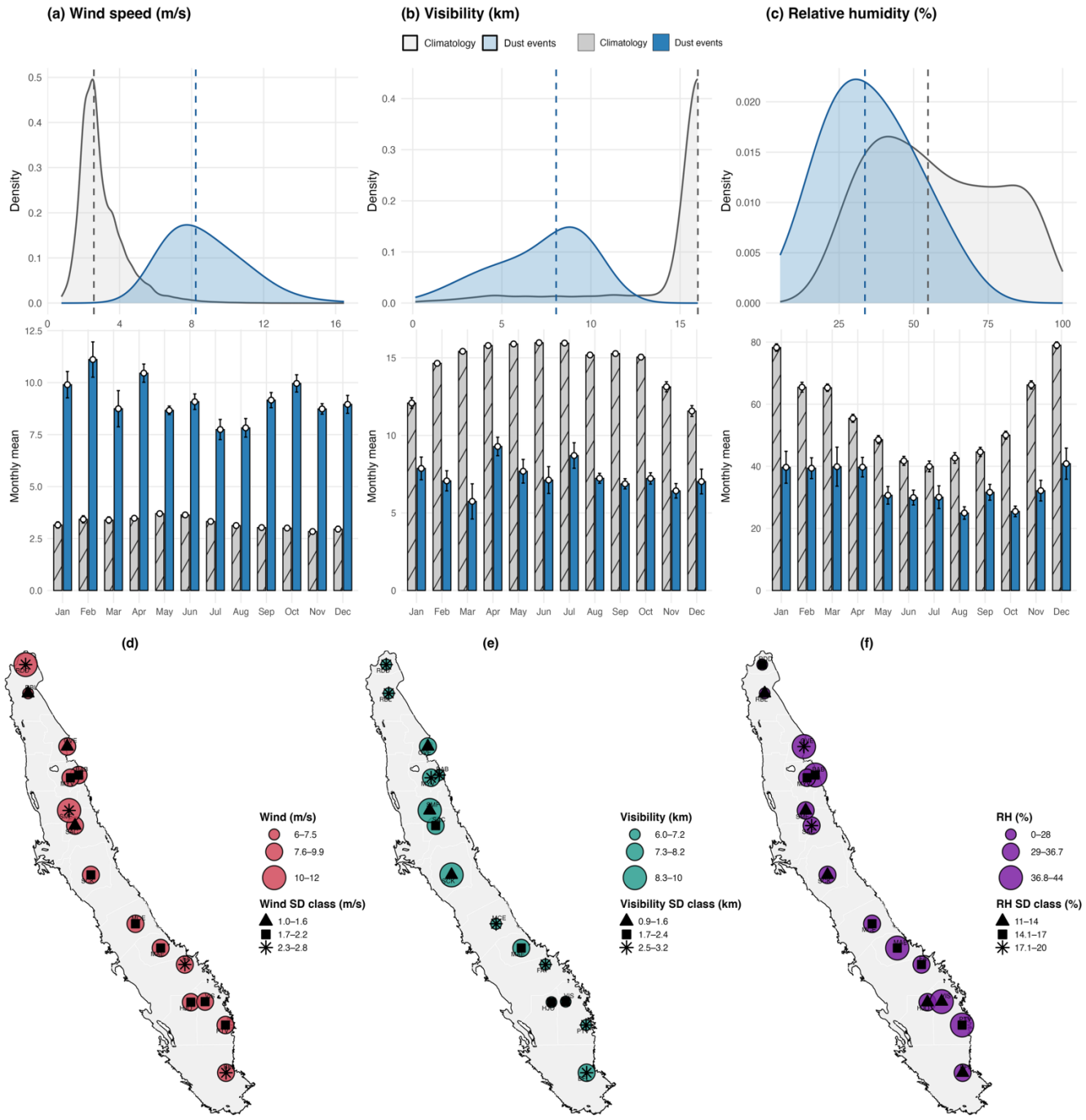

Fig 5. Distributions of meteorological conditions during dust events. (a-c) Probability distributions and monthly means surface wind (m/s), visibility (km), and relative humidity (%) for the dust events (blue) compared to climatology (grey); error bars show variability across the stations. (d-f) Spatial patterns of station mean of surface wind (m/s), visibility (km), and relative humidity (%) during dust events; symbol size encodes magnitude and standard deviation.

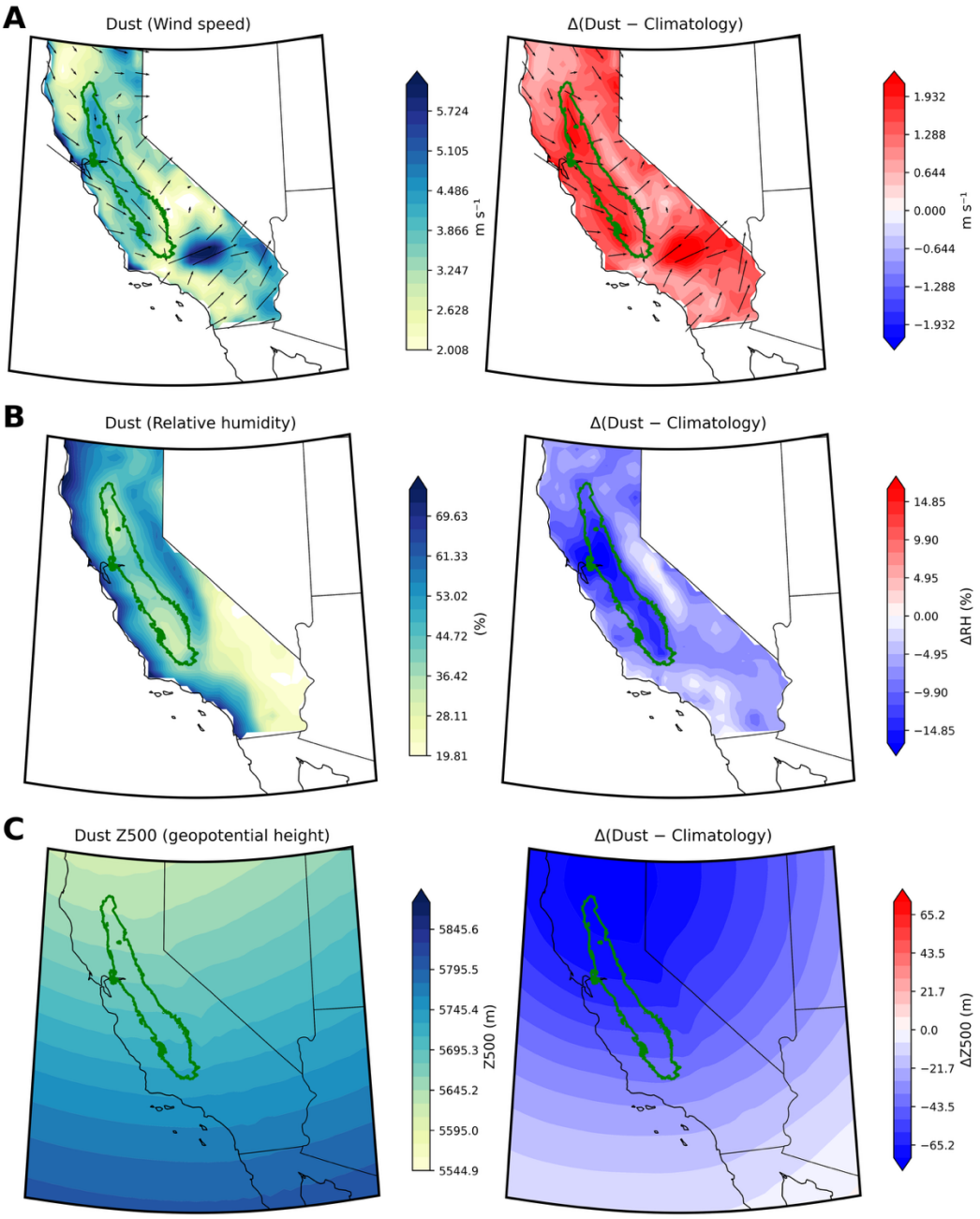

Fig 6. Dust-event composites (left) and anomalies relative to climatology (right) from ERA5 reanalysis. Rows show: (a) 10-m wind speed (m s^{-1}) with 10-m wind vectors, (b) near-surface relative humidity (%), (c) 500-hPa geopotential (Z500, m). The green outline denotes the Central Valley.

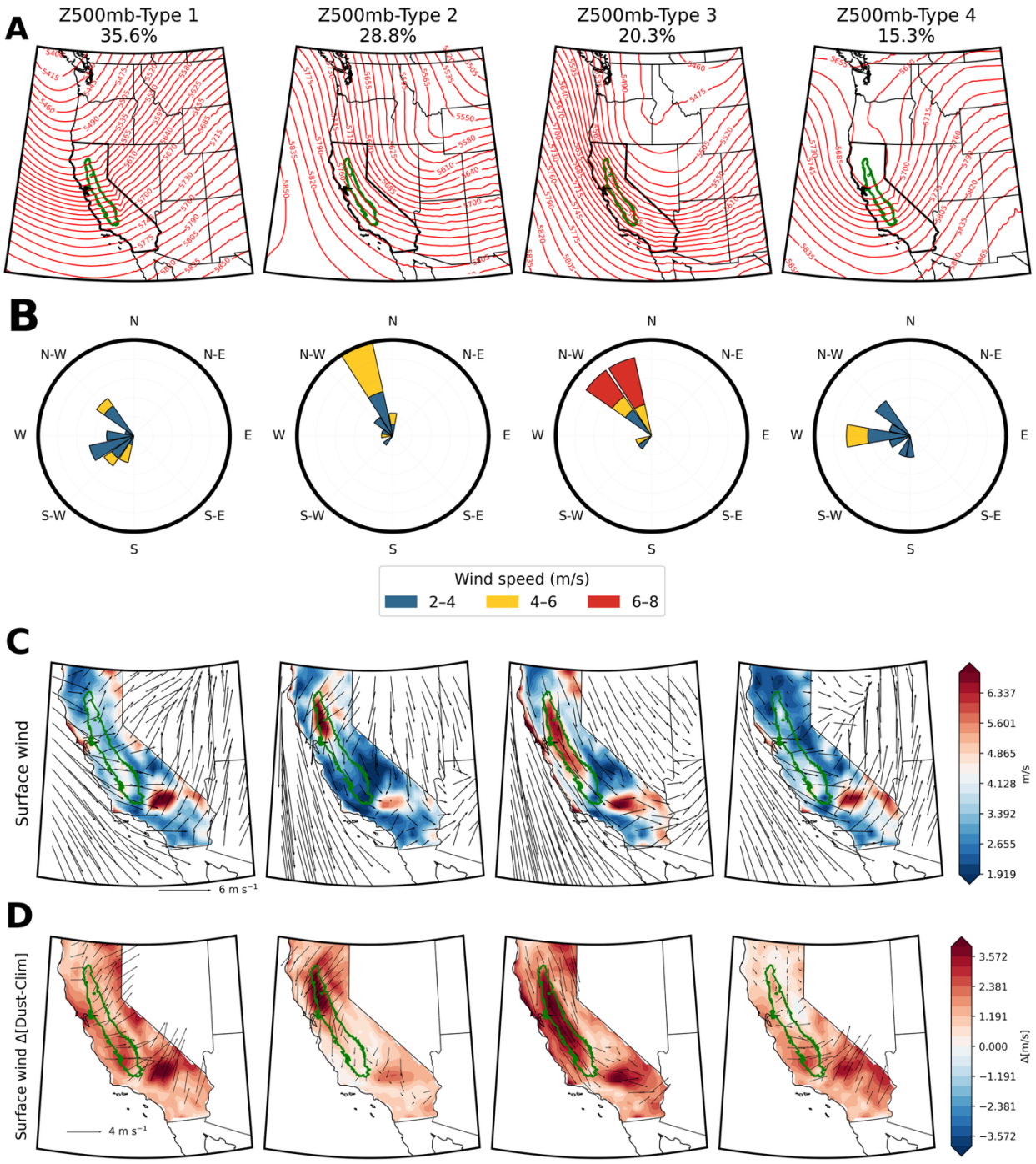

Fig 7. Synoptic configuration pattern during widespread dust event in the Central Valley. (a) SOM composite of 500-hpa geopotential (m) bin into four dominant circulation types with the percentage of dusty days each type represented, (b) wind orientation and speed associated with each Type over the Central Valley, (c) Mean surface wind speed on dusty days for each Type; shading indicates wind speed (m/s) and arrows shows vector direction; (d) surface wind anomalies relative to climatology.

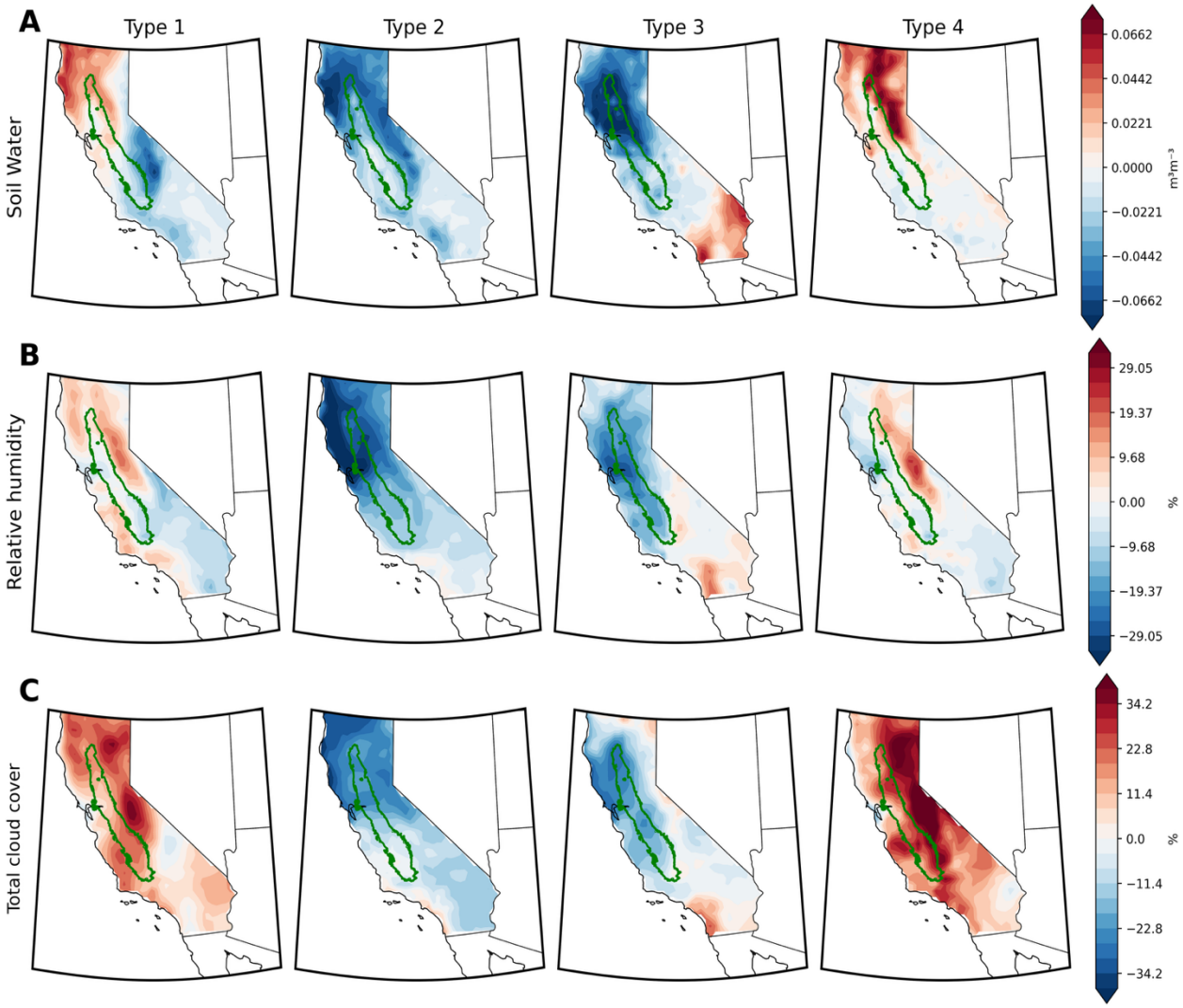

Fig 8. Environmental variables associated with the four dominant circulation types for Central Valley widespread dust events (as identified in Fig 7a). Columns show Type 1 to 4; Rows show composite anomalies relative to the climatology mean for (a) surface soil water (m^3m^{-3}), (b) relative humidity (%), and (c) total cloud cover (%). The green outline marks the Central Valley domain.

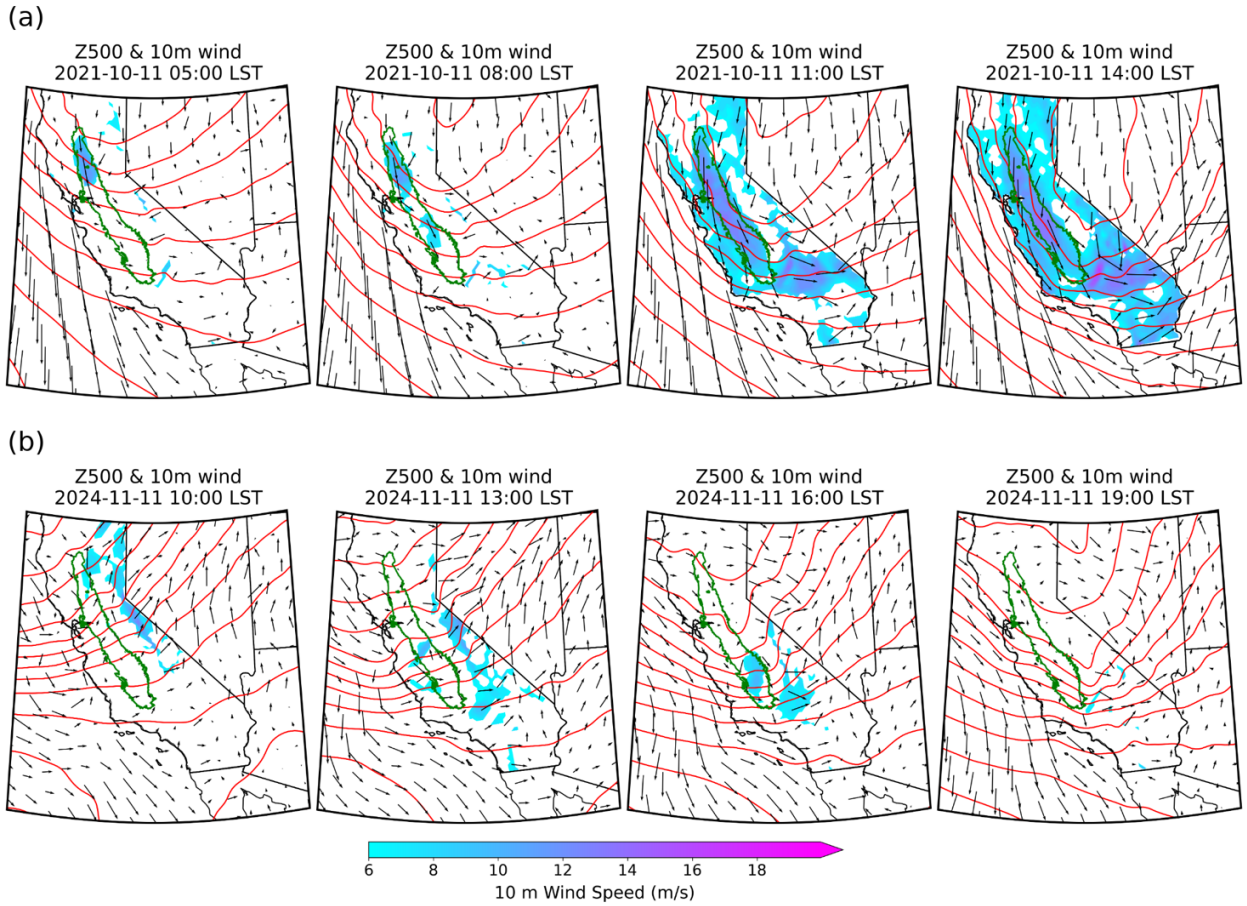

Fig 9. Temporal evolution of synoptic pattern and near-surface wind during two major Central Valley dust events. Panels show 500-hpa geopotential (m; red contours), surface wind vectors (black arrows), and surface wind speed (shading > 6m/s) during October 11, 2021 (top) and November 11, 2024 (bottom) from the RAPv3 dataset. The green outline marks the Central Valley domain.

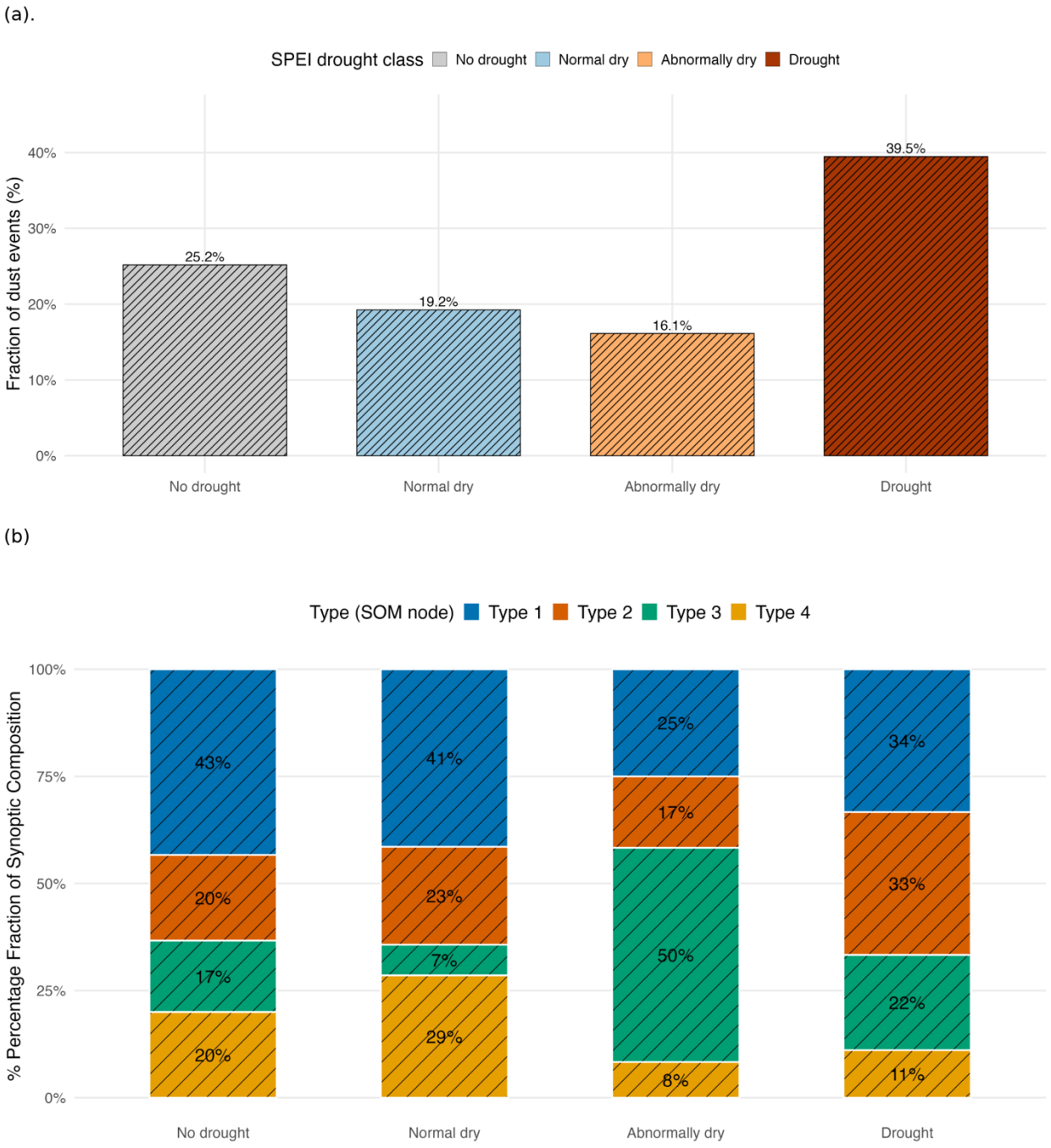

Fig 10. (a) Percentage fraction of dust events as a function of SPEI categories (2005-2024) and (b) distribution of synoptic configurations (as identified in Fig 7a) during dust events across drought. Stacked bars show the percentage fraction of dust events associated with each synoptic configuration/Type as a function of drought severity class.

Supplementary

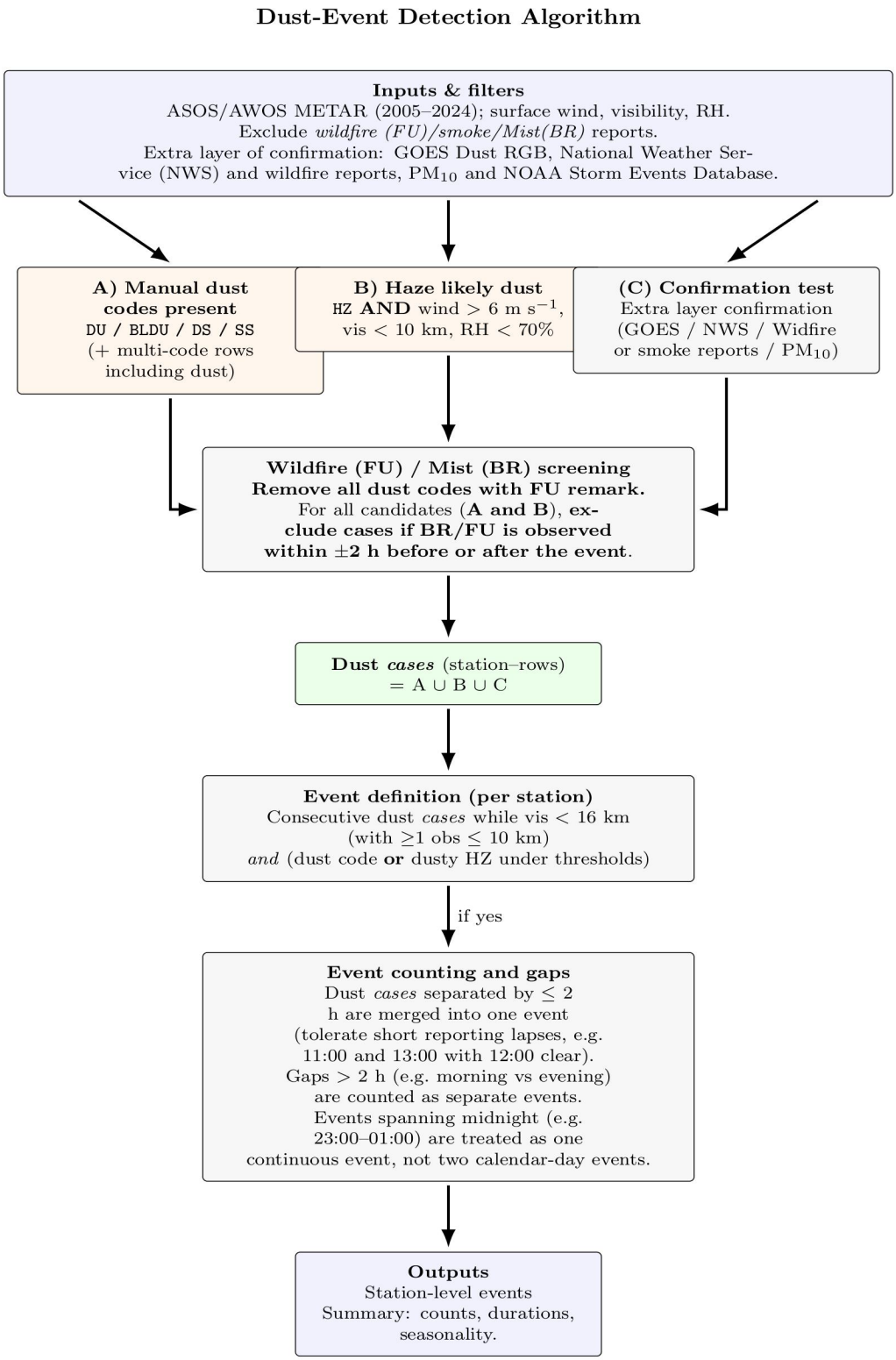

Figure S1. Flowchart showing the procedure used for dust-event identification.

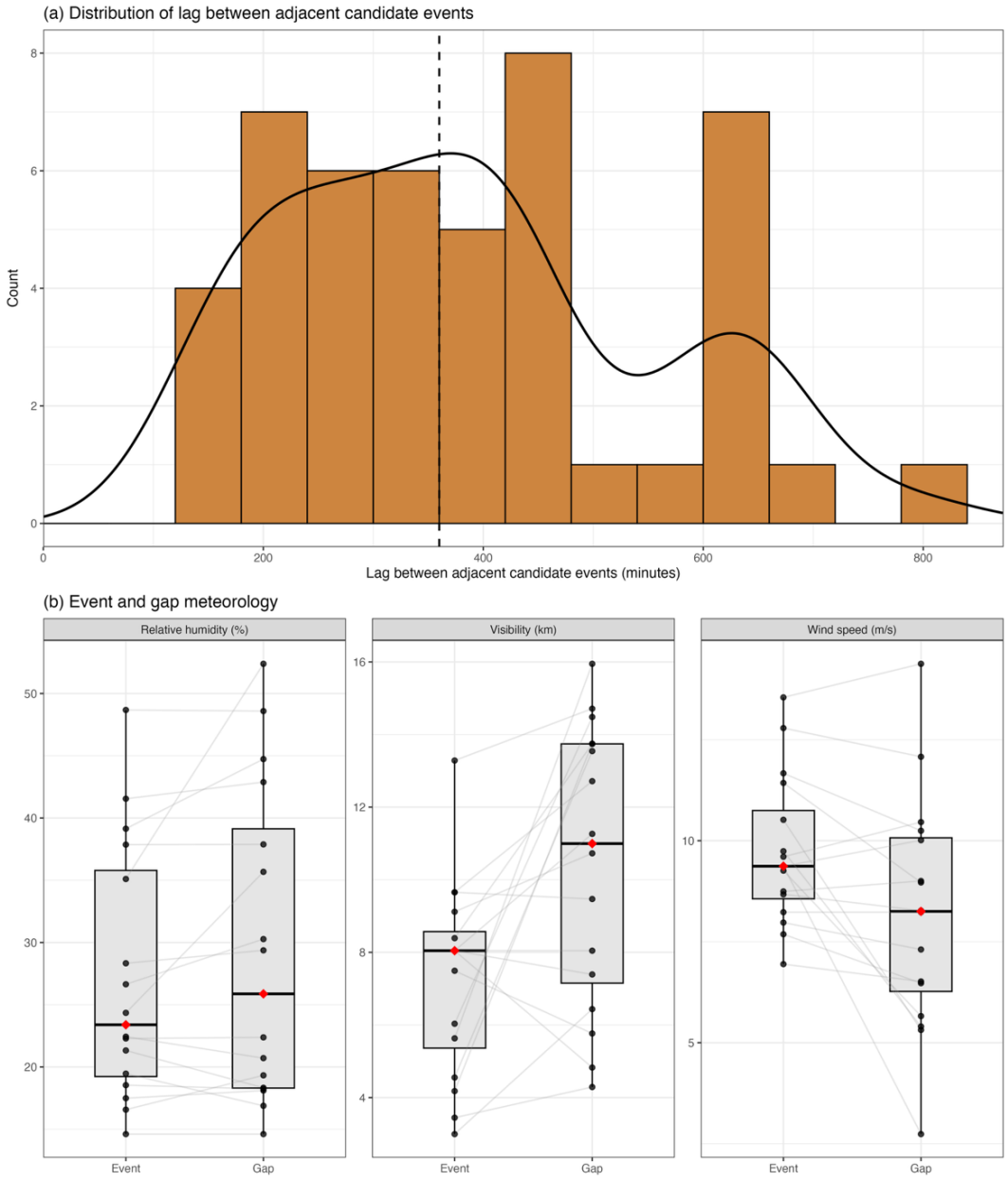

Figure S2: Meteorological characteristics of adjacent candidate dust events (a) Distribution of time lags between adjacent candidate dust events. Dashed vertical line indicates the mean gap period (b) Comparison of meteorological conditions during identified dust events and the intervening gap periods, including relative humidity, visibility, and wind speed. Boxplots show the distribution of events showing the mean and grey connecting lines show paired event-gap comparisons

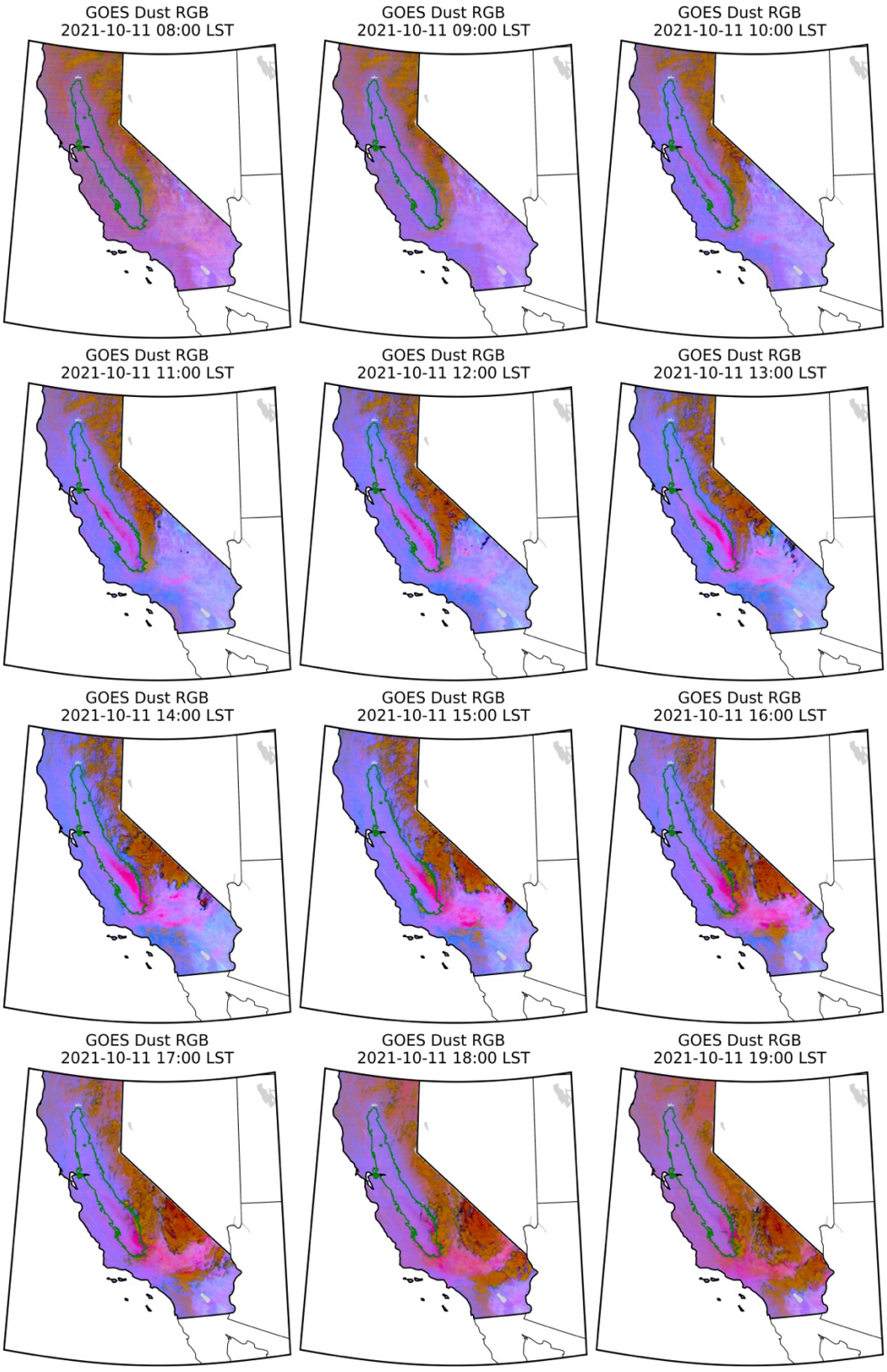

Figure S3. Extended GOES Dust Plume on October 11, 2021.

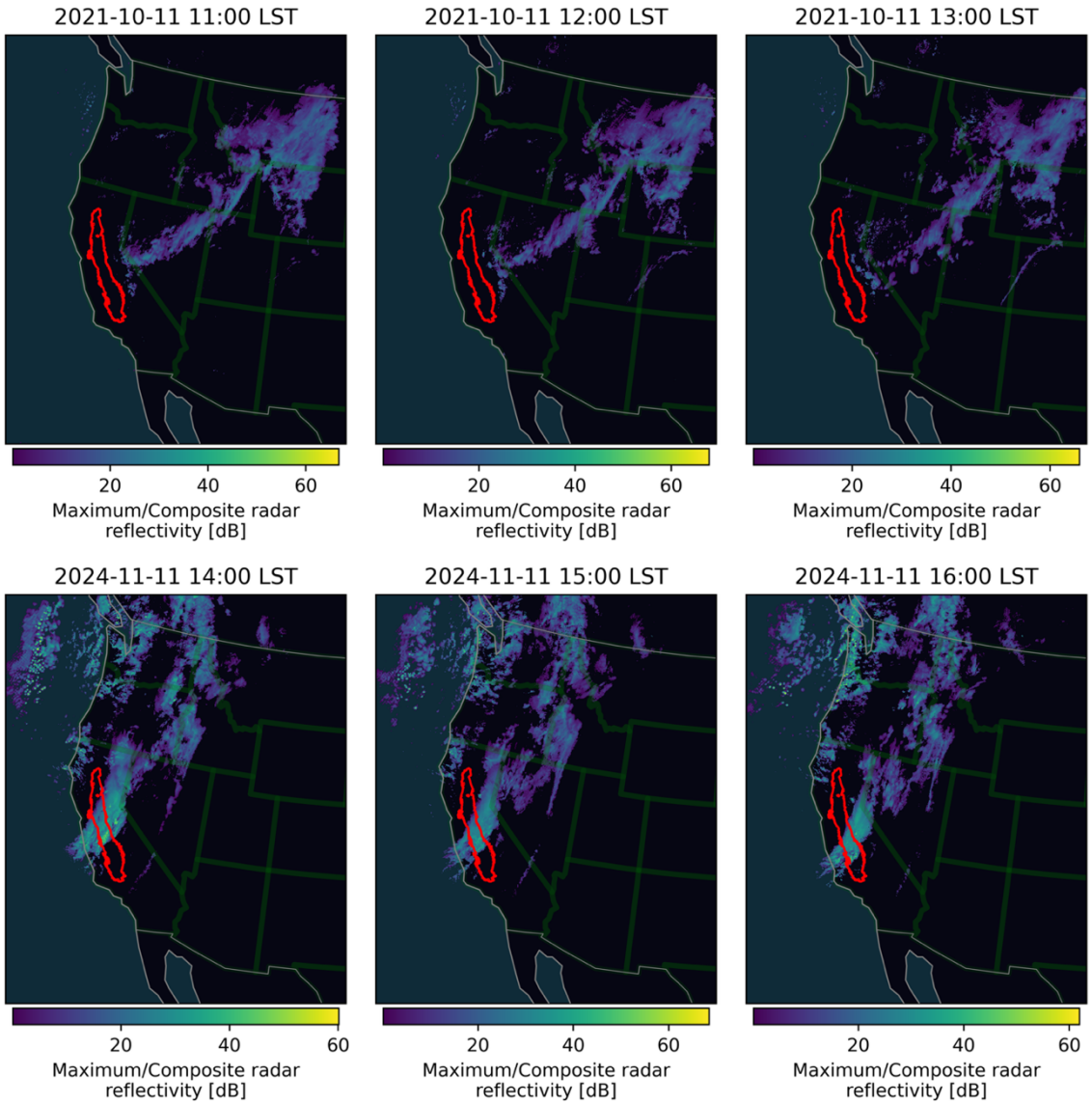

Figure S4. Hourly composite radar reflectivity during two California Central Valley dust events: October 11, 2021 (top) and November 11, 2024 (bottom). The Central Valley dust domain is outlined in red. Times are local standard time (LST).

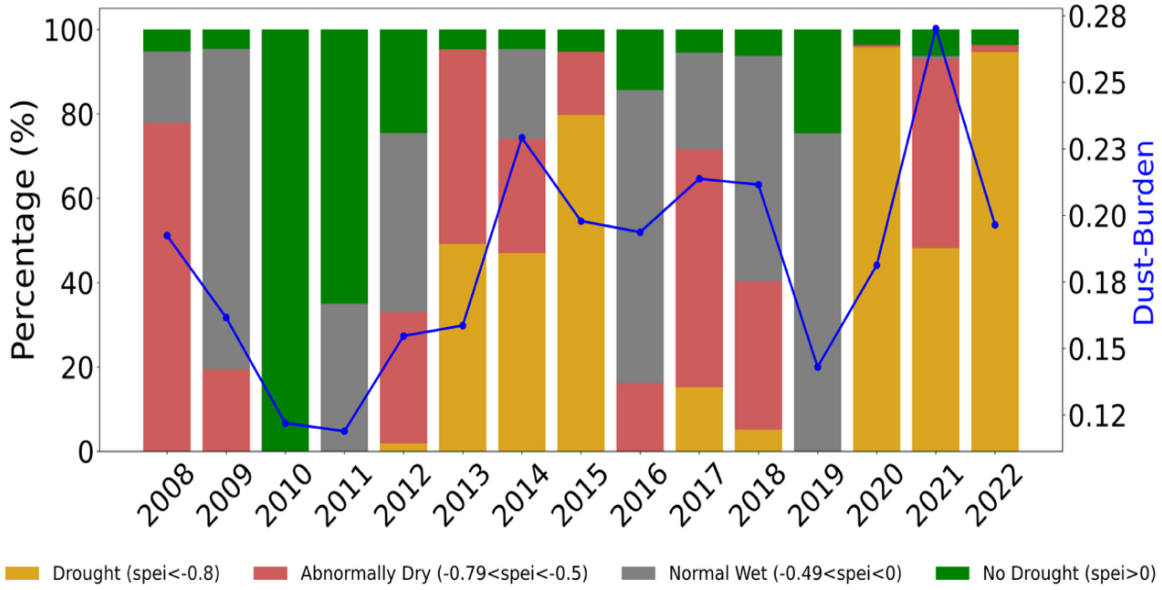

Figure S5. Yearly drought severity class and dust burden in California's Central Valley, 2008-2022. Stacked bars indicating the percentage fraction of SPEI classes per year. The blue line (right axis) is the annual mean dust burden index. Dust burden tends to increase in drought-dominated years (2014, 2015, 2020, 2021). Annual dust events and annual frequency of drought conditions (SPEI< 0) is 0.56 and statistically significant ($p < 0.05$).

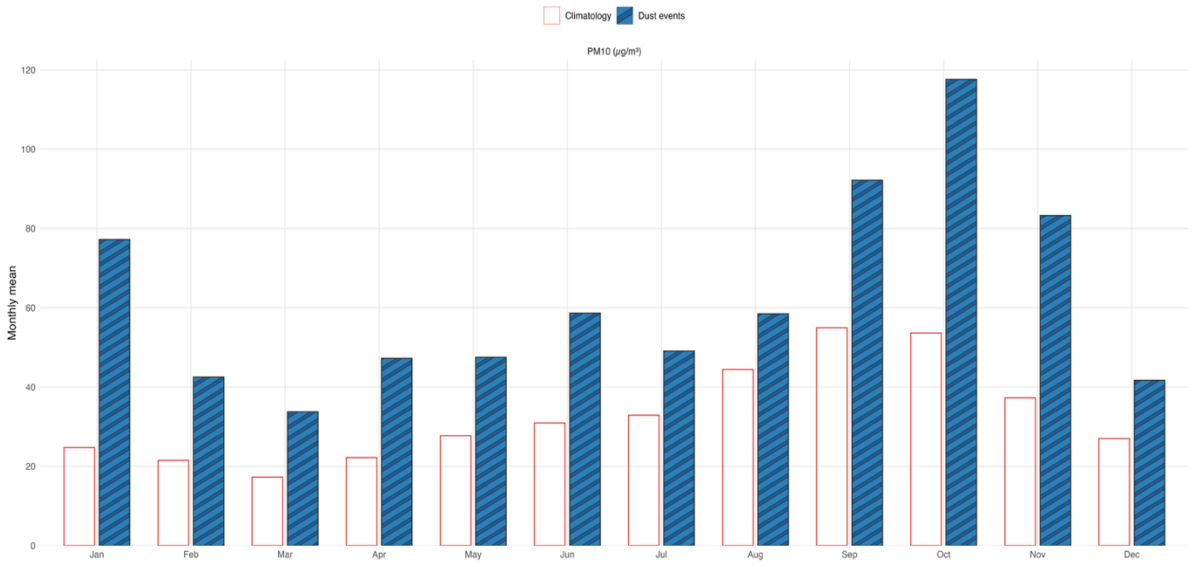

Figure S6. Monthly mean PM10 concentrations ($\mu g m^{-3}$) on dust events (blue bars) relative to climatology mean (red).

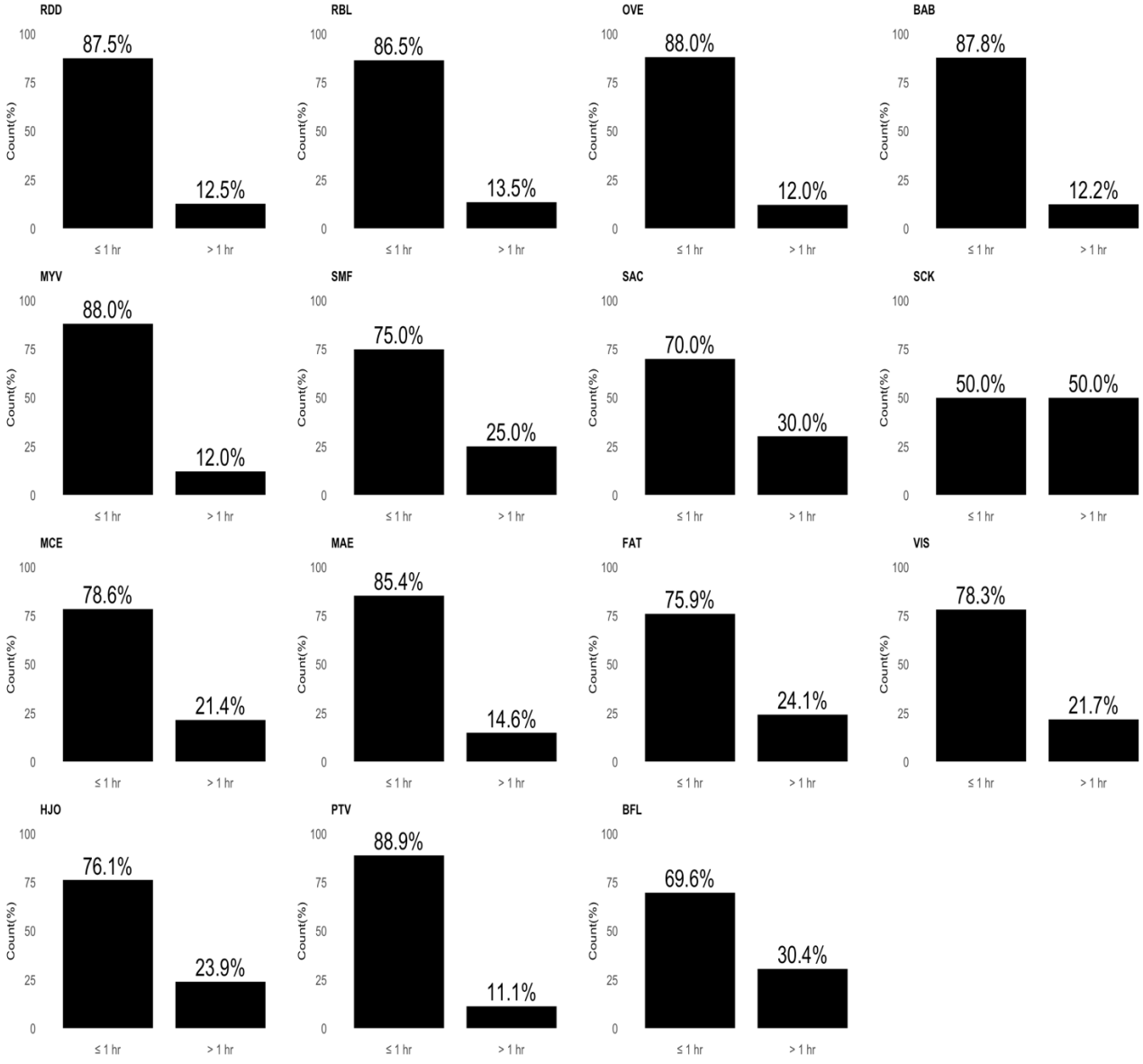

Figure S7. hourly duration of dust event across the Central Valley.

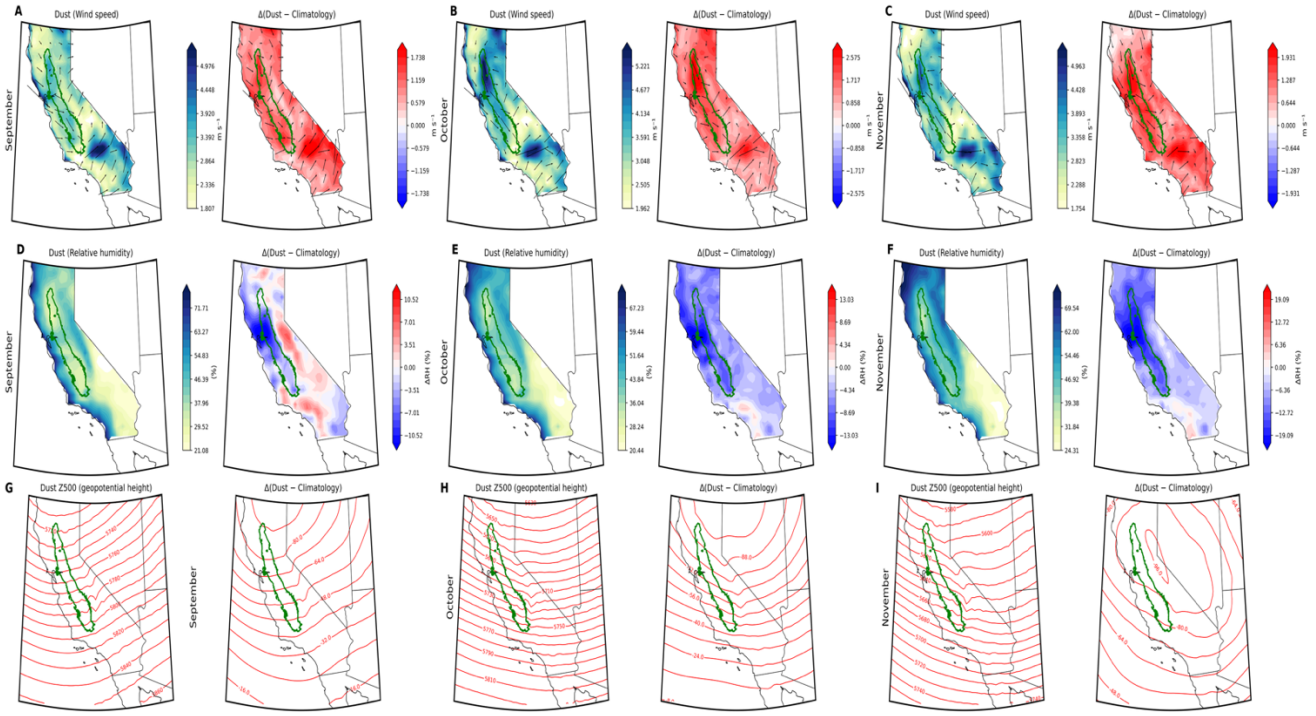

Figure S8. September-November composites of meteorological conditions during Central Valley dust days. For each month (columns), the left subpanel shows the dust day mean, and the right subpanel shows the anomaly relative to climatology. (a-c) surface wind (m/s); (d-f) relative humidity (%); (g-l) 500hpa geopotential (m) (contours). Green outline marks the Central Valley domain.

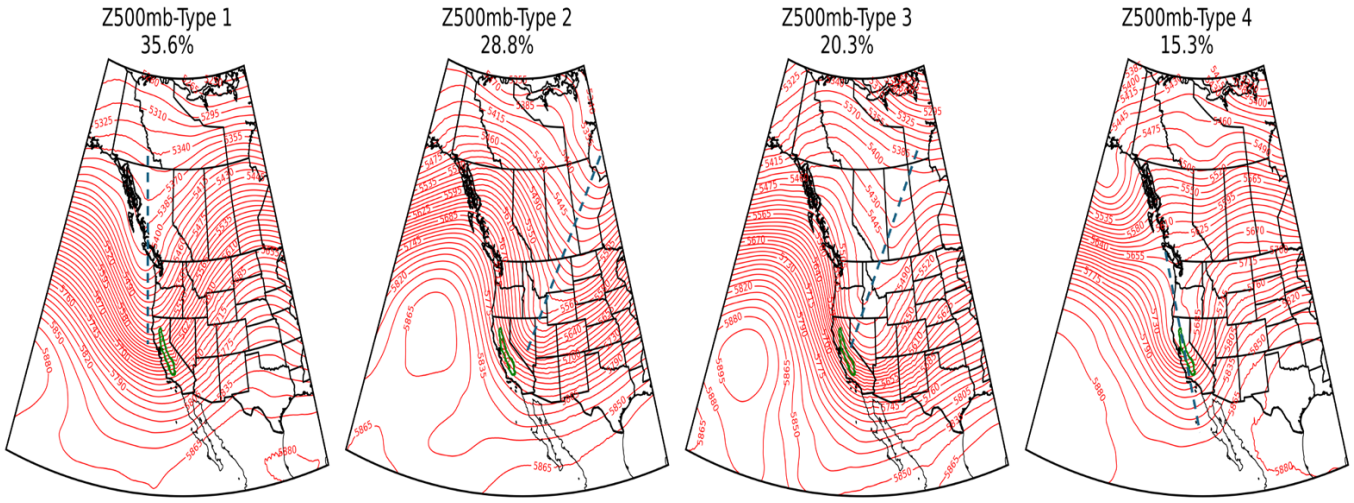

Fig S9. SOM composite of 500-hPa geopotential (m) for the four dominant circulation types associated with widespread dust events

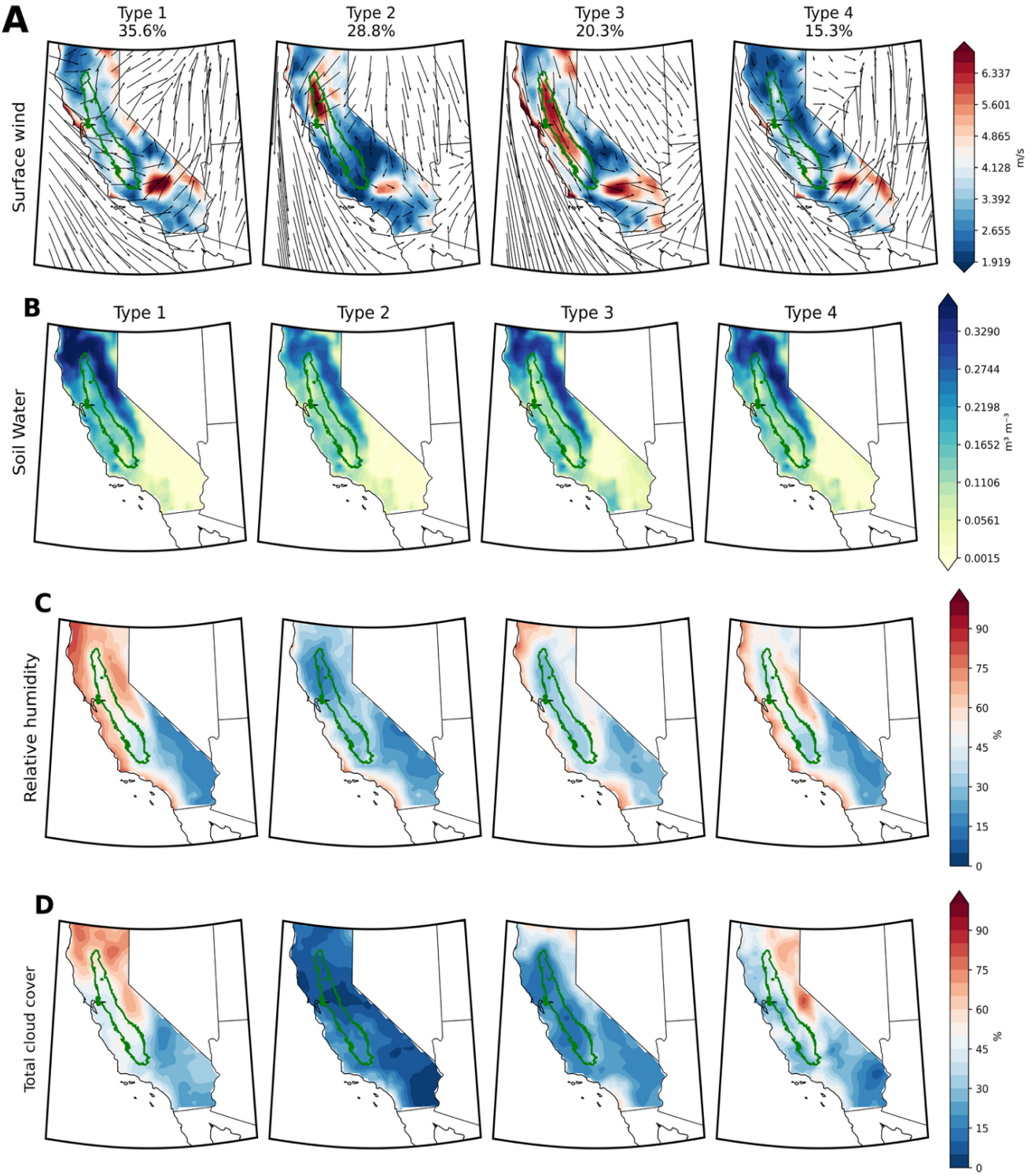

Figure S10. Dust favorable environment associated with four dominant circulation types as identified in fig 7a. Columns show Type 1-4; rows show dust composites mean of (a) surface wind (m/s), (b) surface soil water ($m^3 m^{-3}$) (c) relative humidity (%), and (d) total cloud cover (%). The green outline marks the Central Valley domain.

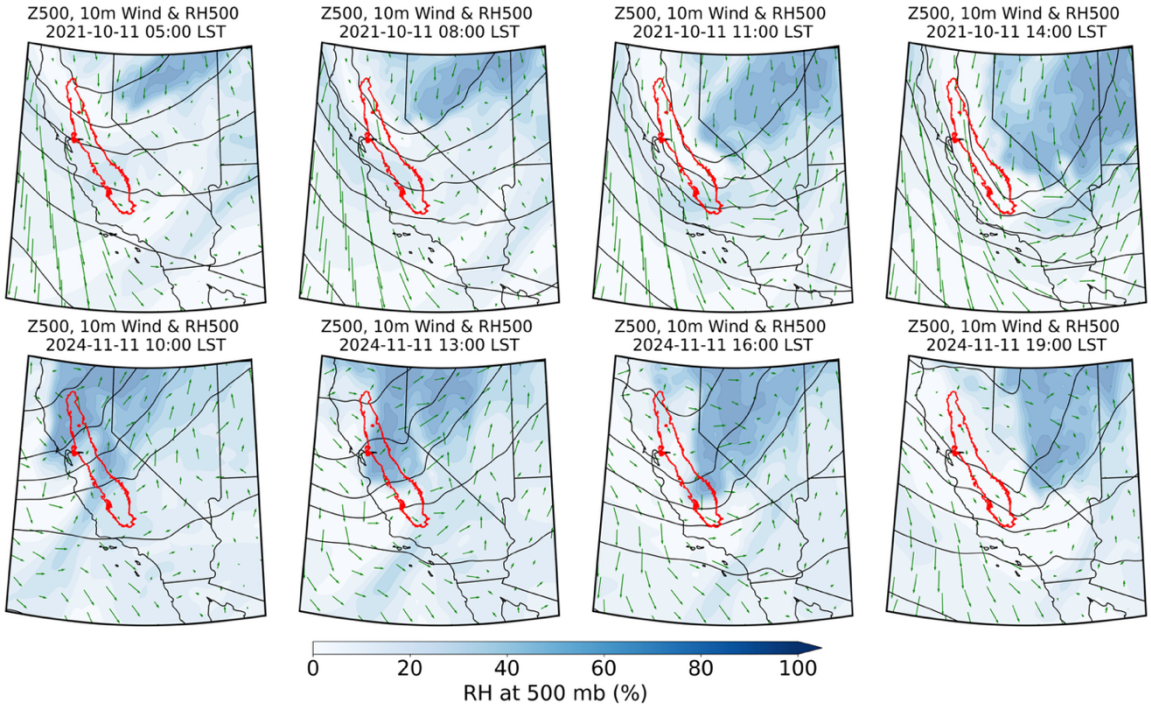

Figure S11. Synoptic evolution of two dust event cases. Panels show 500hpa geopotential (black contours), surface wind vectors (green arrows), and 500hp relative humidity (blue shading) during October 11, 2021 (top) and November 11, 2024 (bottom). The red outline marks the Central Valley domain.

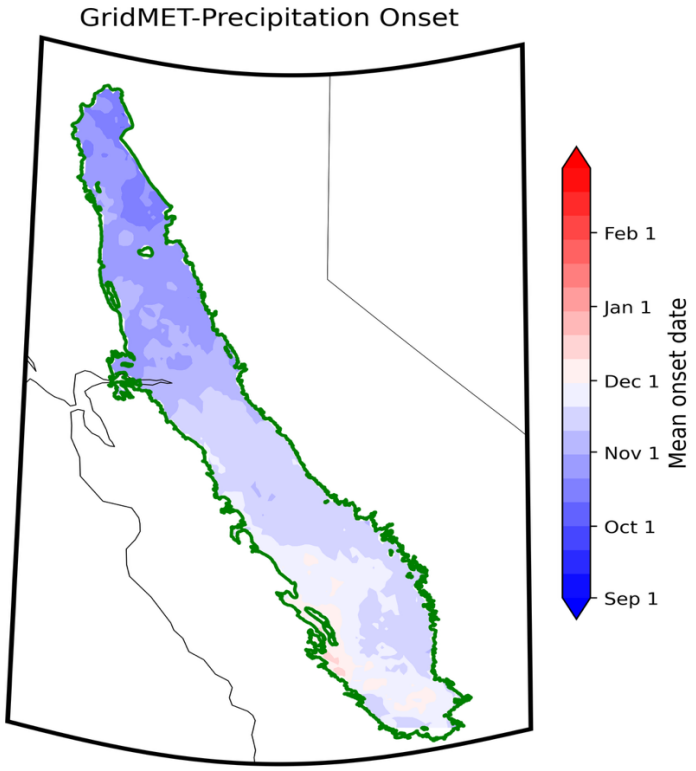

Figure S12. Mean onset date of the first significant rainfall event in the Central Valley (2005-2024).

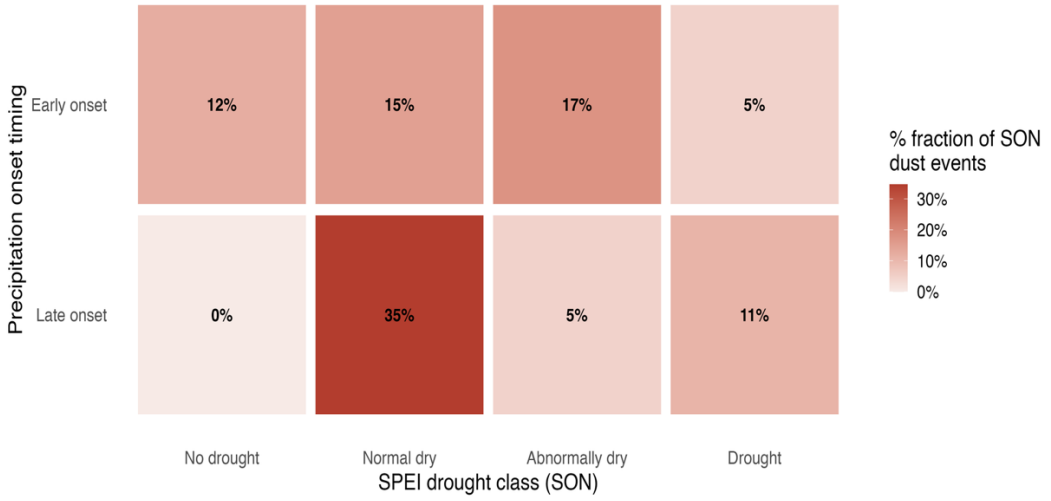

Figure S13. Seasonal modulation of Central Valley dust events during September-November. Panel shows a 2 x 4 grid pairs the Precipitation onset timing (early and late phases) with drought categories. Center values is the % fraction of SON dust events as a function of SON SPEI class (e.g., no drought when SPEI >0; normal dry: -0.49<SPEI<0; abnormally dry: -0.79 <SPEI<-0.50 and drought: SPEI<-0.8)

Table S1. Locations of meteorological stations used in this study.

Station ID	Airport location	ASOS/AWOS	Latitude	Longitude
RDD	Redding Municipal Airport (Redding)	ASOS	40.509	-122.2934
RBL	Red Bluff Municipal Airport (Red Bluff)	ASOS	40.1519	-122.2536
OVE	Oroville Municipal Airport (Oroville)	ASOS	39.49	-121.62
BAB	Beale Air force base (Marysville)	ASOS	39.13609	-121.4366
MYV	Yuba County Airport (Marysville)	ASOS	39.10203	-121.5688
SMF	Sacramento International Airport	ASOS	38.69542	-121.5908
SAC	Sacramento Executive Airport	ASOS	38.5069	-121.495
SCK	Stockton Metropolitan Airport (Stockton)	ASOS	37.89417	-121.2383
MCE	Merced Regional Airport (Merced)	ASOS	37.28603	-120.5179
MAE	Madera Municipal Airport (Madera)	ASOS	36.98486	-120.1107
FAT	Fresno Yosemite International Airport (Fresno)	ASOS	36.78	-119.7194
VIS	Visalia Municipal Airport (Visalia)	AWOS	36.31867	-119.3929
HJO	Hanford Municipal Airport (Hanford)	ASOS	36.31139	-119.6232
PTV	Porterville Municipal Airport (Porterville)	AWOS	36.02732	-119.0629
BFL	Meadows Field (Bakersfield)	ASOS	35.4244	-119.0542

Table S2. Locations of PM10 stations used in this study.

EPA ID	Location	Latitude	Longitude
060311004	Hanford-S Irwin Street	36.314399	-119.64457
061010003	Yuba City (Almond Street)	39.138773	-121.618549
060290014	Bakersfield	35.35661	-119.06261
060195001	Fresno (Clovis Villa Avenue)	36.819449	-119.716433
060392010	Madera (28261 Avenue)	36.953256	-120.034203
060472510	Merced	37.30832	-120.48046
060190011	Fresno Garland	36.78538	-119.77321
060670014	Sacramento (Goldenland Ct)	38.650783	-121.506767
060674001	Sacramento (2221 Stockton)	38.556326	-121.458499
060772010	Manteca (530 Fishback Rd)	37.793392	-121.247874
061072002	Visalia	36.332179	-119.291228